July 2014

Computational Fluid Dynamics Modeling of Karst Conduit-Matrix Exchanges with Relevance to Contaminant Transport and Chemical Reactions

WRRI Technical Completion Report No. 362

John L. Wilson
Katrina M. Henry

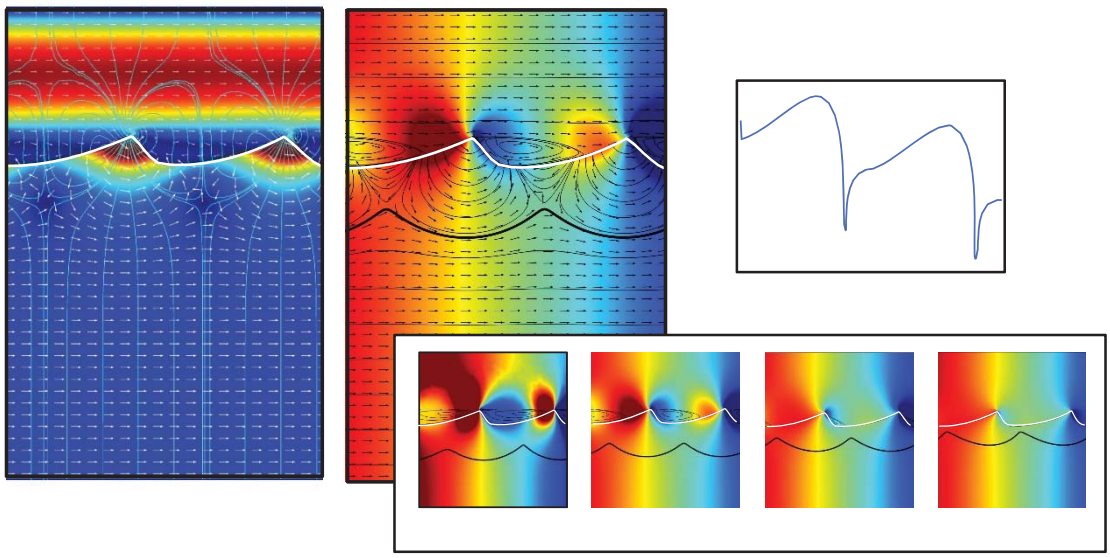

NEW MEXICO WATER RESOURCES RESEARCH INSTITUTE
New Mexico State University
MSC 3167, PO Box 30001
Las Cruces, New Mexico 88003-0001
(575) 646-4337 email: nmwrri@wrri.nmsu.edu

COMPUTATIONAL FLUID DYNAMICS MODELING OF KARST CONDUIT-MATRIX EXCHANGES WITH RELEVANCE TO CONTAMINANT TRANSPORT AND CHEMICAL REACTIONS.

By

John L. Wilson, Professor of Hydrology
Katrina M. Henry, Graduate Assistant
Department of Earth and Environmental Science, Hydrology Program,
New Mexico Institute of Mining and Technology

TECHNICAL COMPLETION REPORT
Account Number 118598

July 2014

New Mexico Water Resources Research Institute
in cooperation with
New Mexico Institute of Mining and Technology

The research on which this report is based was financed in part by the U.S. Department of the Interior, Geological Survey, through the New Mexico Water Resources Research Institute.

DISCLAIMER

The purpose of the Water Resources Research Institute (WRRI) technical reports is to provide a timely outlet for research results obtained on projects supported in whole or in part by the institute. Through these reports the WRRI promotes the free exchange of information and ideas and hopes to stimulate thoughtful discussions and actions that may lead to resolution of water problems. The WRRI, through peer review of draft reports, attempts to substantiate the accuracy of information contained within its reports, but the views expressed are those of the authors and do not necessarily reflect those of the WRRI or its reviewers. Contents of this publication do not necessarily reflect the views and policies of the Department of the Interior, nor does the mention of trade names or commercial products constitute their endorsement by the United States government.

ABSTRACT

In fluvial systems, the hyporheic zone is the subsurface volume where water enters from the stream, travels through the subsurface, and returns to the stream. It is a mixing zone that dynamically changes over space and time because of variations in channel geometry and roughness, streamflow regime and discharge, and other properties and forcings. The fundamental fluid dynamics of karst conduits are not different from streams. Karst conduits have the same features that cause hyporheic flow in fluvial systems. Karst-conduit hyporheic exchange, and related (bio)geochemical processing, then becomes a fundamental component of the karst water cycle. We present computational fluid dynamics models of karst hyporheic exchange. The conduit morphology driving the modeled hyporheic flow is that of a wall scallop and spatial variation in conduit area. The depth of hyporheic flow into the karst matrix surrounding the conduit increases with the flow rate in the conduit, and the size of the morphology driving the flow. Modeling of the residence time of matrix hyporheic exchange indicates the flow can be important for a variety of biogeochemical processes in the karst conduit-matrix system, as well as for contaminant sequestration and transformation.

Keywords: karst, spring, conduit, hyporheic, computational fluid dynamics

Contents

List of Figures

List of Tables

1 Background

Groundwater flow in karst aquifers includes flow in the karstic matrix, for example a carbonate, and flow in conduits, enlarged by dissolution, that puncture the matrix. It is known that fluid flow can exchange between karst matrix and conduits over large spatial scales, with most historic emphasis on flow from matrix to conduit. What has not been previously recognized is that fluid exchange can also occur over very small spatial scales, induced by local fluid pressure variations along the conduit wall caused by wall morphology and conduit sinuosity. In analogy to a similar exchange between streams and fluvial aquifers, we call this 'karst-conduit hyporheic exchange'. This exchange may have significant implications for the natural chemical evolution of karst waters and the reactive chemistry of contaminants.

1.1 Hyporheic Flow in Fluvial Systems

The Hyporheic Zone. Surface streams concurrently gain and lose water along their course via the hyporheic zone (Bencala, 1993; 2011), as illustrated in Figure 1. Traian Orghidan, a Romanian hydrobiologist and biospeleologist, created the term 'hyporheic' from Greek words *hypo* ($\upsilon\pi o$, under) and *rhe* ($\rho\epsilon$, flow or current) (Orghidan, 1955; Smith, 2005; Dahm et al., 2006)[1]. Therefore, the most literal definition of a hyporheic zone is the region where flow of surface water occurs under a stream (below the water table). There are a variety of more refined definitions, based on academic discipline (Smith, 2005). Ecologists, who are prolific publishers on hyporheic exchange, describe the zone as the area between the stream and groundwater that is biologically active (Boulton et al., 1998). Hydrologists often define the zone as the area below and to the side of the stream where surface stream water and

[1]Hyporheic flow is first described in Orghidan (1955), followed by the well known German language version Orghidan (1959). There is a recent English language translation of the article, Orghidan (2010).

groundwater mix (Sophocleous, 2002). Geochemists have defined the hyporheic zone as the area where 10% to 98% of the subsurface water came from the stream (Triska et al., 1989). There is not yet a unified definition of a hyporheic zone that cross cuts disciplines (White, 1993; Gooseff, 2010). This report describes hyporheic exchange primarily from a hydrological perspective. Therefore, we define a fluvial hyporheic zone as the zone where stream water enters the sediment, mixes with groundwater, and then returns to the stream.

Importance of Hyporheic Exchange in Fluvial Systems. It has only been in the last couple of decades that this hydraulic coupling between stream and groundwater has been recognized as a fundamental process affecting the chemistry and biology of streams, and the transport and transformation of stream nutrients and contaminants (Salehin et al., 2004). This recognition has revolutionized that science, with related articles increasing exponentially in the last 25 years (Dahm et al., 2006; Bencala, 2011). Hyporheic exchange, which occurs in both gaining and losing streams (Malcolm et al., 2009), is caused by small-scale (local) pressure or head gradients produced by sediment morphology and heterogeneity, channel sinuosity, turbulent flow, and others; see Tonina and Buffington (2009) for a review. Storm events are not the primary driver of hyporheic exchange; hyporheic exchange occurs even in steady flow (where stream discharge is not changing). Two fundamental aspects of hyporheic exchange are its dynamic nature and variety of scales: hyporheic exchange is dynamically changing in space and in time due to variations in channel geometry and roughness, streamflow regime and discharge, the heterogeneity of aquifer properties, mobile sediments, and the spatial and temporal variation of other properties and forcings (Elliott and Brooks, 1997; Buffington and Tonina, 2009).

1.2 Background on Karst Aquifers

Importance & Properties of Karst Aquifers. Karst aquifers supply about 25% of the world's population with water (Ford and Williams, 2007), including nearly all the drinking water to certain regions, for example 90% of Florida's drinking water (Paulson et al., 1990). The presence of conduits is a hallmark of many karst aquifers. Conduits are regions of converging or diverging flow with fast flow rates and are thus analogous to streams (White, 1988; Field, 1988; 1993). Phreatic conduits are connected, water-saturated tubes (below the water table) from one centimeter to tens of meters in diameter that contain most of the flow in the aquifer but less than 5% of the storage (Atkinson, 1977; Budd and Vacher, 2004). Most phreatic conduit flow is turbulent (White, 2002; White and White, 2005). Surrounding the conduit is water-saturated matrix rock that contains little of the aquifer flow (essentially all of it Darcian), but comprises most of the aquifer volume and hence most of the storage (Worthington et al., 2000). Fractures are ubiquitous in karst; they transmit water faster than the matrix, and slower than conduits. Most conduits are formed from fractures (Palmer, 2007).

Fluid Exchanges in Karst Aquifers. The conceptual model of fluid exchange during baseflow conditions is of water in the karst matrix entering the conduit, or perhaps moving from matrix to fracture to conduit (White, 1988). This matrix to conduit movement has been well established with geochemical and dye tracer tests. During a flood, conduit water may enter the matrix, as observed with geochemical measurements (Martin and Dean, 2001; Ritorto, 2007; Moore et al., 2009; Bailly-Comte et al., 2010) and modeled for a generic conduit (Wilson and Henry, 2014). Smaller scale exchanges from conduit to matrix during base-flow conditions have not yet been observed. This is not surprising as the analogous hyporheic flow in streams was not observed until the 1950s (Orghidan, 1955).

2 Description of Hyporheic Flow in Karst Systems

2.1 Hyporheic Exchange in Karst Systems

We suggest that, as for streams, conduits are not pipes (Bencala, 2011). With hyporheic exchange, conduits concurrently gain and lose water all along their course, whether or not there is a large-scale net gain or loss of water along the length of the conduit, or no net exchange (Cardenas, 2009). This is not a reach of conduit temporally switching over time between gaining and losing, but a continuous small scale exchange whether the conduit is gaining, as illustrated in Figure 2a, losing (Figure 2c), or has no net exchange with the matrix (see Figure 2b). A cut-away model of karst hyporheic flow at the margin of a karst conduit is shown in Figure 3.

A conceptual model of conduits functioning as something other than pipes allows for mixing between conduit water and the matrix, bringing together dissolved minerals, organic carbon, nutrients, electron acceptors, and chemical and biological contaminants. The dynamically changing spatial and temporal pattern of this exchange provides an opportunity for reactions to occur in the matrix, often mediated microbiologically, and fed by a supply of new and chemically fresh (or contaminated) conduit water entering the matrix (Hendricks, 1993; Hancock et al., 2005; Haggerty et al., 2009). Constituents, moving quickly through the conduit, are diverted into the slower moving and highly reactive matrix, experiencing a sequence of different conditions, with varying residence times depending on the path taken (Martin and Dean, 2001).

On terminology. The term 'hyporheic exchange' may not be the best descriptor for the small spatial scale, mixed-water flow at the margin of karst conduits. We chose it because this karstic flow has many aspects in common with fluvial hyporheic flow: dynamic temporal

and spatial patterns, mixed waters, and geochemical gradients. However there are important differences between conduits and streams (see §2.5). Because the term karst hyporheic flow invokes the many similarities between the flow at the margin of karst conduits and fluvial hyporheic flow, we have chosen to adopt, and adapt, the word 'hyporheic' to this newly described environment, rather than creating a new descriptor.

2.2 Types of Karst-Conduit Hyporheic Zones

Since we are quantifying hyporheic exchange for a new application of the concept, we present additional definitions. We suggest that karst-conduit hyporheic-zone interactions can be broadly divided into two types: the sediment hyporheic zone (the volume of conduit sediment where conduit water and sediment water mix) and the matrix hyporheic zone (the volume of the matrix where conduit water and matrix water mix). These zones can exist wherever sediment or bedrock, respectively, is in contact with flowing water in vadose caves (located above the water table) and phreatic conduits, as in photographs shown in Figure 4.

2.2.1 Sediment Hyporheic Zone

The sediment hyporheic zone is the region of the sediment, typically lying on the bottom of a conduit, where water from the conduit enters the sediment, moves through the sediment, mixes with sediment water, and returns to the conduit. Since the sediment itself can move though the conduit at short time scales, this region is mobile (Dogwiler and Wicks, 2005). Figure 4a shows a typical vadose cave stream with a sediment bar to the side of the stream. A sediment hyporheic zone should exist in this bar and in the sediment bed lining this stream. In Figure 4b, sediment hyporheic flow should occur in the sediment along the bottom of the phreatic conduit, as well as in the sediment perched on some areas of the walls. The

karst-conduit sediment hyporheic zone is analogous to hyporheic zones in the sediment at the bottom and sides of a fluvial stream.

2.2.2 Matrix Hyporheic Zone

The matrix hyporheic zone is the region of the rock matrix where water from the conduit enters the matrix, moves through the matrix, mixes with matrix water, and returns to the conduit. The pattern of matrix hyporheic flow, which occupies a very small proportion of the total matrix volume (see Figure 2), depends on a variety of conditions in the conduit and matrix. Regions where the matrix rock is in direct contact with the vadose stream in Figure 4a would have matrix hyporheic exchange, as would areas where the sediment cover is thin. In Figure 4b matrix hyporheic flow would occur in areas where there is bare rock at the conduit-rock interface, and in the rock below thin sediment cover. The matrix hyporheic zone would be analogous to a hyporheic zone in a surface-water bedrock stream with thin sediment cover. This stream-bedrock hyporheic zone has not been well studied (see §4.2 for details).

2.3 Mechanisms of Karst-Conduit Hyporheic Flow

Hyporheic flow associated with fluvial streams and karst conduits is caused by small scale pressure gradients, which make it more efficient for some flow to traverse through the surrounding porous media rather than the open channel (Smith, 2005) or conduit, respectively. For fluvial streams the causes of hyporheic flow that induce these local pressure gradients are well studied and include ripples, dunes, meanders, and differences in the conductivity of the porous media at the margin of the stream (Buffington and Tonina, 2009). Karst conduits have the same attributes that cause hyporheic flow in surface streams. Illustrations of the causes of both sediment and matrix karst hyporheic flow are shown in Figure 5. Of particular

importance in this report is the spatial variation of near-wall pressure head due to conduit flow over rough wall morphology in karst conduits (Figure 5b), analogous to channel flow over ripple and dune bedforms in sediments. The other important mechanism considered in this report is the effect of spatial variation in conduit area (Figure 5e).

2.4 Karst-Matrix Heterogeneity & Hyporheic Flow

Karst-matrix permeability heterogeneity is an important consideration in karst hydrology (Goldscheider et al., 2007) and should play a role in karst-conduit hyporheic exchange (see Figure 5c). Stream hyporheic studies have shown that factors other than aquifer permeability heterogeneity, such as streambed pressure variation caused by bed topography, have a greater influence on the rate of stream hyporheic exchange (Cardenas et al., 2004). Permeability heterogeneity in both fluvial stream sediments and carbonate matrices has been measured to span orders of magnitude (Budd and Vacher, 2004; Fleckenstein et al., 2006; Niswonger et al., 2008; Engdahl et al., 2010). It is unclear how much karst-matrix permeability heterogeneities, which includes fractures, influence karst hyporheic flow. We believe that it is likely that other features, such as conduit sinuosity (which occurs in 3D in karst conduits) and conduit-wall morphological features (which can be of large size and occur all around the wetted perimeter in karst conduits), that actually drive the hyporheic flow, are generally more important than matrix heterogeneity, just as they are for surface streams. However, this remains an open question.

2.5 Critical Differences between Fluvial Hyporheic Flow and Karst Hyporheic Flow

The analogy between streams and conduits is not exact. Some processes and conditions that occur in streams but not phreatic conduits are:

- *Unconsolidated, Non-Dissolvable Bed.* Streams typically occur in unconsolidated sediment, called most generally 'regolith' a term encompassing dust, soil, and rock fragments. The regolith is not usually subject to chemical dissolution. In contrast, the matrix at the margin of phreatic karst conduits is consolidated and highly soluble, at least in carbonate rock. If water is undersaturated, the matrix can undergo dissolution, both at the pore scale leading to permeability and porosity increases, and more spatially focused macro porosity dissolution, such as retreat of the conduit wall, leading to cave formation. If hyporheic flow is a driver of the dissolution, the increased permeability may lead to a feedback loop resulting in more flow and therefore more dissolution, a condition that has not been described for fluvial hyporheic flow. The end of this feedback loop in a karst matrix would be the dissolution of the morphological feature that gave rise to the hyporheic flow.

- *Bioturbation.* Bioturbation and biological alteration of the channel is common in fluvial systems, including by large animals, but is much less common in karst conduits that have lower populations and diversity of lifeforms, including micro-invertebrates. Bioturbation can occur at a smaller spatial scale in phreatic karst-conduit sediments (with the exception of cave divers). In the karst-matrix hyporheic zone bioturbation is not a factor, although microbes may cause significant porosity and permeability changes inside the immobile matrix rock. In surface streams and karst-conduit sediments, microbes and their biofilms are disrupted by flooding, bedload transport, and even bioturbation

by higher life forms; this is not an issue in the rock matrix.

- *Free Surface vs. Conduit Ceiling.* Water in surface streams and vadose caves has a free surface (air-water boundary) for a top boundary. The lack of a free surface in phreatic karst conduits means that the conduit water interacts with the water saturated matrix rock at all its boundaries: floor, sides, and ceiling. To borrow terminology from fluvial systems, the wetted perimeter is a maximum and the hydraulic radius is a minimum in phreatic conduits. The large wetted perimeter in phreatic karst conduits provides additional morphological features that can cause the pressure gradients that drive hyporheic flow.

- *Solar Radiation.* Water in surface streams is subject to direct and diffuse solar radiation and often undergoes diel biogeochemical cycling (de Montety et al., 2011). These diel signals are likely absent in karst conduits, which, a short distance from the entrance, are in darkness; they have no direct or indirect solar radiation. The absence of thermal signals is another consequence of the lack of solar radiation.

- *Water Aeration.* Water in surface streams (and streams in vadose caves) has a free surface (air-water interface) that allows vapor and gas exchange between the stream water and the atmosphere. In contrast, water in phreatic conduits is surrounded by water saturated matrix rock. Because of the free surface, stream water is constantly aerated via turbulent diffusion, agitation from wind, and by water movement over obstacles, therefore oxygen, carbon dioxide, and nitrogen gases are easily exchanged between the stream and the atmosphere. In particular, oxygen, so very important to the biogeochemistry and ecology of streams, is easily replaced by aeration in surface streams but not in phreatic karst conduits.

- *Wind.* Atmospheric wind can lead to additional mixing of dissolved chemicals and gases in streams; phreatic karst conduits do not experience wind.

- *Atmospheric Precipitation.* Surface streams receive atmospheric precipitation directly, as well as through runoff from surrounding landforms and from groundwater upwelling, while karst conduits have no direct input, although they too experience runoff events and groundwater discharge from the matrix.

- *Primary Production.* Water in streams is an important habitat for primary producers or autotrophs, as well as consumers or heterotrophs. Due to the lack of solar radiation, vadose cave streams and phreatic conduits do not have photoautotrophs and represent a heterotrophic end member for stream metabolism. (Simon and Benfield, 2002).

- *Decomposers.* Surface streams can receive leaf fall and other inputs of organic matter leading to a direct input of particulate and dissolved organic matter for decomposition. Phreatic karst conduits must have this material carried in from sinking streams and karst skylights.

- *Riparian Zone.* Bounding a surface stream on its banks is a riparian zone with a unique ecology, including small to large scale photosynthetic vegetation and a variety of animals including vertebrates. The riparian zone of a stream acts as a biologically active buffer or transition zone between the surrounding land cover and the stream. This supplements the stream hyporheic transition zone located below ground. If there is a halo of influence within the karst matrix (adjacent to phreatic conduits but extending beyond the hyporheic zone) that is analogous to a stream riparian zone then its ecology and processes should be very different

3 Implications of Karst Hyporheic Exchange

3.1 Karst Hyporheic Exchange is a Fundamental Component of the Karst Water Cycle

The exchange between conduit water and the rock matrix hyporheic zone is a fundamental component of the karst water cycle and related biogeochemical processes. Characterizing and quantifying the exchange is critical to a complete description of a karst aquifer. The hyporheic zone is an intermediate zone between the conduit water and the matrix water, consisting of mixed waters from both sources. When conduit water enters the hyporheic zone, dissolved constituents, which were moving quickly through the conduit, are diverted into the slower moving and highly reactive matrix of the hyporheic zone, experiencing a sequence of different conditions with varying residence times depending on the path taken (Martin and Dean, 2001). Thus water in the hyporheic zone has a chemistry and residence time distribution in between that of the two end members of conduit water and matrix water. Although the hyporheic zone may be a small volume of the total matrix, because hyporheic flow is faster than flow in the matrix (but slower than in the conduit), and because the extent of the hyporheic flow includes the conduit floor, sides, and ceiling, a large percentage of conduit water can pass through the hyporheic zone if the matrix permeability is sufficiently large. Hyporheic zone water and its local matrix can then undergo processes missing in both the conduit and matrix, including secondary porosity and permeability development leading to speleogenesis, geochemical and biogeochemical cycling, and contaminant processing and transport.

3.2 Secondary Porosity and Permeability Development

In fluvial systems, hyporheic exchange mixes water of different chemistries (Bencala, 2011). In karst systems where the conduit water is chemically different from matrix water, hyporheic exchange produces a mixed water environment in the porous media of the hyporheic zone. The mixed water can be chemically aggressive and cause matrix dissolution (Palmer, 2007), which leads to heterogenous secondary permeability development with regions of enhanced porosity and permeability inside the matrix. This type of permeability development in the matrix surrounding a conduit has been observed in at least one system, although it was not attributed to karst hyporheic flow (Florea, 2006).

3.3 Geochemical Cycling

Stream hyporheic zones are regions of geochemical cycling through redox reactions; about half the nitrogen and phosphorous entering a surface stream, as well as much of the dissolved organic carbon (DOC), can be utilized or retained in the hyporheic zone (Behrendt, 1996; Fiebig, 1995). In karst conduits the fast flow rates and well-mixed water do not allow for redox cycling to occur. In the rock matrix, away from a conduit, a fresh supply of water may not be available. It is in the karst hyporheic zone, with intermediate flow rates and input of chemically fresh conduit water, where geochemical cycling is likely to occur.

Biogeochemical Cycling. Portions of major and minor geochemical cycles are microbially mediated (Pusch et al., 1998). Although the metric for a high trophic state is primary production via autotrophs, in aquatic ecosystems heterotrophic activity can exceed primary production (Dodds and Cole, 2007). In surface streams the fluvial hyporheic zone increases heterotrophic metabolism (Mulholland, 1997). The hyporheic zone is so important to bio-

geochemical cycling in streams that it has been referred to as "the river's liver" (Fischer et al., 2005). If heterotrophic activity is sufficiently abundant then significant biogeochemical cycling can occur in the karst hyporheic zone. Previous studies of trophic activity in karst conduits or the karst matrix may not adequately describe the tropic activity in the previously unidentified karst hyporheic zone.

3.4 Contaminant Transport

Dynamic hyporheic flow activates and deactivates matrix contaminant reservoirs. The dynamically changing spatial and temporal pattern of karst hyporheic exchange may activate and deactivate contaminant reservoirs residing in the matrix or sediment adjacent to the conduit. This dynamic exchange may explain the temporal variability often observed in karst conduit discharge at, for example, springheads, where some contaminant concentrations increase during storms while others decrease (Mahler and Massie, 2007; Vesper and White, 2006; Vesper, 2008). Hyporheic exchange may also interact with dense non-aqueous phase liquids (DNAPL) contaminants that are assumed to be located below the sediment of a conduit, and hence out of direct conduit flow (Loop and White, 2001). A recent focus group on karst resources stated that "How and when contaminants are stored and transported in karst systems is not well understood ... questions that need to be addressed relative to contaminant transport are: ... 2) the exchange of water and solutes between the matrix, fracture, and conduit permeability zones; ... Closely related is the need to understand where contaminants are stored in the aquifer, particularly if they are immobile." (Vesper and Schindel, 2008). The fact that contaminant storage and transport in karst aquifers cannot be completely described indicates there are one or more underlying processes that are not well understood, and perhaps not even recognized. Karst-conduit hyporheic flow, which provides a continuous flux between the conduit and matrix, and switches scales with the conduit flow regime, thus

activating and deactivating different reservoirs in the matrix (Figure 6), can help explain the incongruous behavior of contaminants in karst aquifers. In fluvial systems the movement and sequestration of contaminants is a well established consequence of fluvial hyporheic flow (Gu et al., 2007; Fritz and Arntzen, 2007; Kazezyilmaz-Alhan, 2008; Landmeyer et al., 2010).

Contaminant attenuation and transformation via biotic processes. The previous discussion of geochemical cycling also applies to contaminant transformation in the karst-conduit hyporheic zone. Stream hyporheic zones host significant natural remediation of contaminants (including nutrients, metals, and organic chemicals) in which a balance is struck between relatively slow water movement through the hyporheic zone and a supply of new and chemically fresh and/or contaminated channel water entering the matrix (Hendricks, 1993; Hancock et al., 2005; Haggerty et al., 2009). The same balance exists for karst conduits. Many of the contaminants of concern in karst conduits are also natural chemical constituents, such as nitrogen, which have been introduced to the aquifer in excessive quantities by anthropogenic activities (Katz et al., 2004). Biogeochemical cycling in the karst hyporheic zone is the only significant process that can transform these chemicals in conduit water, provided there is a sufficient source of DOC, prior to karst waters discharging at a spring or well.

4 Previous Work on Karst-Conduit Hyporheic Exchange

4.1 Laboratory Experiments

About 40 years ago, a series of steady-flow, permeable pipe laboratory experiments were conducted by fluid dynamicists at MIT (Olsen and Eckhert, 1966; Munoz Goma and Gelhar, 1968; Chu and Gelhar, 1972; Ho and Gelhar, 1973; 1974; 1983). The purpose of the experiments was to observe and describe flow analogous to that in porous alluvial channels

and, although not specifically mentioned, hyporheic zones and karst conduits. In effect, they were the original laboratory hyporheic zone experiments, although the authors never extrapolated the results to a natural system with exact geometric similitude. Because they chose to run their experiments in pipes, in effect they created idealized karst conduits with permeable walls (see Figure 7). Some experiments had straight permeable pipes, while others had permeable wavy bedforms. The permeable wavy bedform experiments, as in Ho and Gelhar (1973), showed that the bedforms caused a phase shift of the pressure distribution in the tube. The phase shift was dependent on Reynolds number, and the permeability, amplitude, and wavelength of the bedforms. Compared to experiments with wavy impervious pipes, the variations of mean velocity profile and turbulence distribution were dependent on the mean flow, especially in areas where the pipe was widening. Though not their intent, these experiments demonstrate that the fluid dynamics of hyporheic flow in streams (gravity flow) and phreatic conduits (pressurized flow) are governed by the same governing equations, the Navier-Stokes equations and Darcy's law.

More recent experiments were conducted by karst hydrologists at Florida State University (Li, 2004; Li et al., 2008; Faulkner et al., 2009). These experiments demonstrated conduit to matrix flow in small physical models (essentially 2D) of unconsolidated matrix material with a screened conduit. While an excellent first attempt, these physical models did not preserve geometric or dynamic similitude for a conduit in a karst aquifer.

4.2 Bedrock Stream Hyporheic Zones

Karst matrix-conduit hyporheic exchange it is analogous to bedrock-stream hyporheic exchange. A logical question is then: what research has been conducted on hyporheic flow in bedrock streams? After an unproductive search of the literature, we contacted Ellen Wohl,

a leading bedrock stream hydrologist/geomorphologist (Wohl, 2010a). She replied "I think that there are certainly two hyporheic zones, in the alluvial cover and in the shallow bedrock, as you mention. I presume that the shallow bedrock one is less important in most cases, although it might be quite important if alluvium is minimal and the bedrock is densely jointed and/or has a highly permeable matrix – we just do not know" (Wohl, 2010b). This suggests that research on the karst-conduit hyporheic zone should also provide findings of interest for bedrock-stream science, particularly for streams flowing over permeable sandstones, limestones, and volcanics.

4.3 Modeling Fluvial Hyporheic Zones

There have been many mathematical model studies of stream hyporheic zones, where the hyporheic flow is driven by pressure gradients due to morphology. Most models of bedform-driven flow examine only the hyporheic zone, applying an assumed pressure fluctuation at the top of the sediment (bottom of the water column in the stream), usually assumed to be sinusoidal in space (see Cardenas and Wilson (2007a) for review). Other models simulate both the channel flow and underlying hyporheic flow, using the channel model to derive pressures along the top of bedforms that are then used to drive the Darcian hyporheic flow in the underlying sediments (Cardenas and Wilson, 2007a; c). Using this approach, there have been a suite of modeling efforts examining the influence of hyporheic exchange on sediment temperature (Cardenas and Wilson, 2007b), reactive chemistry, and hyporheic-zone residence time distributions (Cardenas et al., 2008). There is even a model of the effects of stream ice cover on the hyporheic flow in underlying sediments (Cardenas and Gooseff, 2008). The ice cover influences the hyporheic exchange, which is greater in magnitude but reaches a shallower depth into the sediment. These coupled stream-porous media models are all 2D in cross-section and assume steady flow.

This report presents a similar 2D, steady flow modeling approach for karst hyporheic flow, in which the conduit flow is first modeled to derive pressures at the conduit wall, that are then used to drive karst-conduit hyporheic flow in the adjacent matrix. The geometry is similar to the ice-covered stream case, with no-slip boundary conditions at the top and bottom of the water column, suggesting that we should find a similar result for karst conduits where pressure fluctuations are driven by wall morphology on the conduit ceiling as well as the floor (and sides).

5 Project Objectives

5.1 Objectives

The project objective was to explore, through mathematical modeling, conduit-matrix water hyporheic exchange in karst aquifers with zero net exchange, see Figure 2b. Specifically, three modeling goals were:

1. *Multiphysics Modeling of Phreatic Karst-Conduit Hyporheic Flow.* Construct 2D, longitudinal cross-sectional multiphysics models of karst-conduit hyporheic flow using COMSOL MULTIPHYSICS. These models use the multiphysics feature of COMSOL with laminar flow in the conduit and Darcian flow in the matrix, and describe the extent and rate of hyporheic exchange as a function of wall morphology, conduit size, conduit flow rate, and matrix hydraulic conductivity.

2. *Turbulent Flow in the Conduit.* These models build off of the previous multiphysics models, using COMSOL's turbulent flow capability for the conduit.

3. *Residence Time Distributions.* Develop a multi physics model that performs tracking

of matrix groundwater-age and incorporate it into the two previous COMSOL flow models to measure the residence time of hyporheic exchange. This is the first step toward future reactive transport modeling of the matrix and hyporheic zone, and it provides information relevant to geochemical cycling and contaminant sequestration and transformation.

5.2 Success

5.2.1 Modeling Goals

Modeling goals 1 & 3 were met. The methods, results, implications, and recommendations pertaining to these goals are described in the remainder of this document. Modeling goal 2 was not met. The software used to complete the models, COMSOL MULTIPHYSICS, was unable to perform accurately the turbulent modeling of conduit flow. After dialoging with COMSOL tech support in the United States and Sweden, the software developer confirmed that the turbulent flow multiphysics would not work for our problem. The budgeted amount for this section of the work was returned to the WRRI.

5.2.2 Funding

Another metric of success was securing additional funding to continue this work. Based, in part, on the results of this seed WRRI grant, we have recently been awarded an NSF grant to continue the modeling work and to attempt to observe hyporheic flow at the margin of actively flowing phreatic conduits and paleo karst conduits (air filled caves) in Florida. This NSF project started on April 1, 2012, with NSF Award Number 1141768. The total award is $261,540. In addition, a PhD student working on the project received a 3-year EPA STAR

Fellowship to continue work on this topic.

5.2.3 Presentations & Publications

The following presentations were made describing work produced from this grant:

> Henry, K., Wilson, J., and Kincaid, T. (2011). Experimental design of a dye trace from conduit to matrix. *Geological Society of America Abstracts with Program*, 43(5):290

> Henry, K. and Wilson, J. L. (2011b). Residence times of karst conduit hyporheic flow. *Geological Society of America Abstracts with Program*, 43(5):341

> Henry, K. and Wilson, J. L. (2011a). Karst hyporheic exchange below conduits with turbulent flow. *Eos Transactions, AGU, Fall Meeting Supplement*, pages H23F–1333

Shortly after the submission of this report the results herein, along with supplemental material will be submitted to a peer reviewed journal as:

> Henry, K. and Wilson, J. (2014). Karst-conduit hyporheic exchange. *Hydrology & Earth System Science*, in preparation

6 Methods

6.1 Mathematical Framework

6.1.1 Navier-Stokes Equations Describe Laminar Conduit Flow

The governing equations for laminar conduit fluid flow are the Navier-Stokes (Navier, 1822; Stokes, 1845) and continuity equations. Other phenomenological laws have been used to describe conduit fluid flow, such as the Darcy-Weisbach equation, but they are approximations derived from observations, not physical law (Streeter and Wylie, 1983). The Navier-Stokes equations are conservation of momentum equations applied to Newtonian fluids; that is, fluids for which stress is linearly proportional to strain rate (the constant of proportionality is the fluid viscosity) (Beckie, 2005). For an incompressible fluid with constant viscosity, the Navier-Stokes equations are (Furbish, 1997):

$$\frac{\partial \mathbf{u}}{\partial t} + \mathbf{u} \cdot \nabla \mathbf{u} = -\frac{1}{\rho} \nabla p + \nu \nabla^2 \mathbf{u} \tag{1}$$

where $\mathbf{u}$ is fluid velocity [$\mathrm{m\,s^{-1}}$]; ρ is the fluid density [$\mathrm{kg\,m^{-3}}$]; p is the fluid pressure [$\mathrm{kg\,m^{-1}\,s^{-2}}$]; and ν is the kinematic viscosity of the fluid [$\mathrm{m^2\,s^{-1}}$]. These three equations have four unknowns. The continuity equation (Furbish, 1997):

$$\nabla \cdot \mathbf{u} = 0 \tag{2}$$

is incorporated to form a closed system of equations. With defined boundary conditions the Navier-Stokes equations can be used to model fluid flow in a conduit. For steady flow, the first term in Equation 1 goes to zero.

6.1.2 Darcy's Law Describes Matrix Flow

Flow in a consolidated or unconsolidated porous medium is described by Darcy's law (Darcy, 1856). Although Darcy's law was originally phenomenologically defined, it is a conservation of momentum equation that can be derived from the Navier-Stokes equations (Equation 1). The generalized form of Darcy's law, for a fluid of constant density, is given by (Bear, 1979):

$$\mathbf{q} = -\mathbf{K}\nabla h \tag{3}$$

where $\mathbf{q}$ is the Darcy velocity or specific discharge [$\mathrm{m\,s^{-1}}$]; $\mathbf{K} = \mathbf{k}\rho g/\mu$ is the hydraulic conductivity tensor [$\mathrm{m\,s^{-1}}$]; $\mathbf{k}$ is the intrinsic permeability tensor [$\mathrm{m^2}$]; g is gravitational acceleration [$\mathrm{m\,s^{-2}}$]; $\mu = \nu\rho$ is the fluid dynamic viscosity [$\mathrm{kg\,m^{-1}\,s^{-1}}$]; $h = p/\rho g + z$ is the hydraulic head [m]; and z is elevation [m]. Note there is no variable in Darcy's law differentiating consolidated porous media (e.g. matrix) and unconsolidated porous media (e.g. sediment). Therefore, the simulations in this work are equally valid for matrix, sediment, or a combination thereof -as long as the other variables (e.g. permeability, porosity, geometry, etc.) are the same across the porous media. The simulation results below assume that conductivity and permeability are both homogeneous and isotropic scalars, so that $\mathbf{K} = K$ and $\mathbf{k} = k$ are both constants. The continuity equation for constant fluid density and porosity (incompressible fluid and non-deformable porous media), or for steady flow, is (Bear, 1979):

$$\nabla \cdot \mathbf{q} = 0 \tag{4}$$

6.1.3 Groundwater-Age Equation Describes Hyporheic Zone Residence Time

A groundwater sample consists of water parcels that have resided in the subsurface for different lengths of time (Bethke and Johnson, 2008). The time the parcel has spent in the subsurface is its 'age' (Kazemi et al., 2006). For karst-conduit hyporheic flow we set the water age to zero when it leaves the conduit and enters the matrix. The age then represents the time that water parcel has been in the hyporheic zone. We use the age concept to calculate hyporheic zone residence time, mathematically represented by the age of water as it leaves the hyporheic zone and returns to the conduit.

The most complete description of groundwater-age gives the exact age of each water parcel in the sample. That is, it gives the distribution of groundwater ages in a sample. Mathematically this type of age distribution formulation has been described in general by Rotenberg (1972), applied to groundwater hydrology by Ginn (1999), and modeled by Gomez and others (2012). Keeping track of age distribution is computationally difficult, therefore groundwater-age is often described by a simpler formulation, average age. The average age is the mean age of all the water molecules in a sample. This is conceptually intuitive but age is an intensive property (i.e. scale invariant), which leaves no method to allow for mixing of groundwater samples of different volumes (Bethke and Johnson, 2008). A computational simple, scalable groundwater-age dating method is given by Goode's (1996) description of the 'age mass' of water samples. Age mass [s kg] is the product of the mean age [s], volume [m^3], and fluid density [$kg\,m^{-3}$] (Goode, 1996). Age mass is an intensive quantity that is conceptually and mathematically analogous to solute mass. Therefore, age mass, like solute mass, is conservative and undergoes storage, advection, diffusion, and dispersion (Bethke and Johnson, 2002). For steady flow in a 2D, homogeneous domain, an age mass transport equation is (Goode, 1996):

$$\frac{\partial \tau}{\partial t} = \nabla \cdot \mathbf{D} \nabla \tau - \mathbf{v} \cdot \nabla \tau + 1 \tag{5}$$

where τ is the age mass [s kg]; $\mathbf{D}$ is the hydrodynamic dispersion tensor [$m^2\,s^{-1}$]; $\mathbf{v} = \mathbf{q}/\theta$ is the seepage velocity vector [$m\,s^{-1}$]; and θ is the effective porosity [-]. The dispersion tensor $\mathbf{D} = D_{ij}$ is defined by Bear (1979) as

$$D_{ij} = \alpha_L |\mathbf{v}| \delta_{ij} + (\alpha_L - \alpha_T) v_i v_j / |\mathbf{v}| + D_m^* \tag{6}$$

where α_L and α_T are the longitudinal and transverse dispersivities respectively [m]; D_m^* is the effective molecular self-diffusion coefficient [$m^2\,s^{-1}$]; and δ_{ij} is the Kronecker delta function [-].

The last term (1) of Equation 5 is the production term [kg]; age mass is continuously generated throughout the domain (for these models the domain is the matrix) at a unit production rate. Water entering the domain (e.g. from the conduit) has an age of zero (Goode, 1996). Age mass is removed from the domain by water leaving the domain through advection, dispersion, and diffusion (Bethke and Johnson, 2002). The mathematical homology between age mass and solute mass can be seen by replacing, in Equation 5, τ with solute concentration, c, and the last term with a zero-order source term; these substitutions transform the age mass transport equation to the solute transport equation. This homology is useful because existing solute transport codes can be used to model age mass.

6.2 Computational Fluid Dynamics

The Navier-Stokes equations do not have a general closed-form solution so Computational Fluid Dynamics (CFD) is used to describe karst hyporheic flow through numerical simulations.

Specifically, approximate steady-state solutions to the Navier-Stokes equations in the conduit, the Darcian flow field in the matrix, and the water age or residence time in the hyporheic zone are found using the finite element method (FEM), a method based on Courant (1943). The finite element software used is COMSOL MULTIPHYSICS.

6.2.1 Physical Domain of the Model

The 2D model domain consists of a longitudinal cross section along the center-line of an essentially straight conduit sandwiched between permeable matrix that is located above the conduit ceiling and below the floor (Figure 3). As depicted in Figure 8a water is assumed to move from left to right, in the positive x direction, with the same mean hydraulic gradient in both the conduit and the matrix. For the model, the main mechanism of hyporheic exchange is the small scale pressure-head fluctuations along the conduit wall caused by non-uniform wall morphology (Figure 5b). The morphology driving the hyporheic flow is that of a scallop (Figure 8a), a common feature found on conduit walls (Blumberg and Curl, 1974). The other important morphology considered in the model is effect of spatial variation in conduit area (Figure 5e).

6.2.2 Finite Element Mesh

The model domain is divided into an array of finite elements. The finite element mesh is generated for the conduit and matrix using COMSOL (Figure 8b). The unstructured nature of the mesh allows for it to have smaller elements at the boundaries, especially at lower radii of curvature or corners. The vertices of each element are nodes; it is at nodes where the solutions of the equations are calculated, the solutions are then interpolated for the rest of the domain. The unstructured finite-element mesh allows FEM models to better model

irregular boundaries such as the complex morphology of a conduit wall. A typical model in this work has 11,330 (19,908) elements and 5,813 (16,737) nodes in the conduit (matrix).

6.2.3 Boundary Conditions & Initial Conditions

Typical boundary conditions applied to the flow model are illustrated in Table 1 for the particular case of a conduit with a porous-matrix floor and ceiling. In some scenarios the ceiling is impervious, as in Figure 8. The steady-state Navier-Stokes model solves for the flow velocities and pressures in the conduit, given a prescribed periodic pressure-head drop across the domain. The laminar (2D cross-sectional) conduit flow rate is given by

$$\frac{b^2}{12\mu}\frac{\Delta p}{L} = \overline{u}_x \tag{7}$$

if the conduit floor and ceiling are both flat, where b is the conduit diameter (height in 2D) [m]; L is the longitudinal length over which the pressure drop occurs [m]; and $\overline{u}_x$ is mean velocity in the conduit x direction [$\mathrm{m\,s^{-1}}$]. By applying appropriate pressure-head drops, $\Delta p/\rho g$, to our more realistic simulated conduit geometries, a range of laminar conduit flow rates are obtained. For example, for the geometry shown in Figure 8 the simulated range is u_x = 0.0 - 0.4 $\mathrm{m\,s^{-1}}$. The conduit pressures, velocities, Reynolds numbers, and other metrics presented later are based on the simulation results for the actual geometries modeled.

The pressure distribution at the conduit-matrix boundary is what is needed to model karst-conduit hyporheic flow in the matrix. The pressure at the boundary is derived from the steady-state solution to the Navier-Stokes equations in the conduit (1, 2) and prescribed as a Dirichlet boundary condition for the wall boundary of the porous matrix (Table 1). The matrix flow field is then computed using the steady-state Darcian model (3, 4) and periodic

Table 1: Boundary Conditions for Conduit and Matrix Flow Models. The Dirichlet BC for the matrix model refers to wall pressures inherited from the conduit flow model.

Model Subdomain	Top & Bottom Boundaries	Left & Right Boundaries
Matrix at Ceiling	No flow above; Dirichlet below	Periodic pressure drop, Δp
Conduit	No slip above; No slip below	Periodic pressure drop, Δp
Matrix at Floor	Dirichlet above; No flow below	Periodic pressure drop, Δp

boundary conditions on the right and left. The model is sequential, that is, the matrix flow field is not used to modify the conduit flow field. This assumption is valid as long as the volume of water entering the conduit from matrix hyporheic flow paths, over the length of the modeled domain, is small compared to the volumetric flow rate in the conduit (Cardenas and Wilson, 2007a; c).

Once the flow field in the matrix is determined, the age distribution of the hyporheic zone in the matrix is computed using (5) and the boundary conditions shown in Table 2. An age of zero is assigned to water entering the matrix from the conduit, §6.1.3. Where water returns to the conduit, the spatial gradient (normal to the wall) of age is set to zero so that only advection carries age mass out of the matrix. The age and age flux entering the left side of the matrix, where ambient groundwater flow enters the model, is set equal to the age and age flux leaving the matrix on the right using a periodic-age boundary condition. In this way, the modeled age represents only the effect of young water entering the matrix from the conduit inside the modeled reach. This age is measured from the time water enters the matrix until it returns to the conduit. The residence time is the time it takes the water to move from one

Table 2: Boundary Conditions for Residence Time in the Matrix

Conduit-Matrix Boundaries	No Flow Boundaries	Left & Right Boundaries
Inflow: τ=0 Outflow: zero age gradient	No age flux	Periodic age flux

end of the hyporheic zone to the other, where it discharges back to the conduit. The spatial distribution of residence time is the mass flux-weighted age returning to the conduit.

6.2.4 Constructing & Running the Model

The model is run in COMSOL by the following steps:

1. *Model Domain Geometry* The model domain geometry is entered into COMSOL as a CAD drawing or using the graphics functions in COMSOL.

2. *Gridding*. The domain is gridded in COMSOL using special routines near corners and other key geometric features. If the finite element mesh is poorly refined near these features, the model may have trouble converging.

3. *Governing Differential Equations & Physical Parameters*. The governing differential equations (Navier-Stokes for the conduit, Darcy's Law and Age Equations for the matrix) and physical parameters (e.g. compressible/incompressible flow, fluid density and viscosity, matrix permeability, porosity, dispersivities, and diffusion coefficient) are set for the domain and subdomains.

4. *Initial Conditions & Boundary Conditions*. The boundary conditions are set (see Tables 1 and 2) and initial conditions (initial guesses) are selected to initiate the equation

solver. The simulations are for steady state conditions, but an initial guess of the conduit fluid velocity and pressure is needed to iteratively solve the non-linear Navier-Stokes equations. Similar initial guesses are also used to iteratively solve the Darcian and age subdomains.

5. *Running the Model*. The model is specified so that COMSOL solves the Navier-Stokes equations (Equations 1 and 2) first, generating the pressure at the conduit-matrix boundary. Next, the flow field in the matrix is solved using Darcy's law (Equations 3 and 4). Finally, the residence times in the matrix are calculated using the flow field in the matrix and Equation 5.

6. *Post Processing*. Generation of figures and plots is completed in COMSOL and/or MATLAB.

7 Results and Discussion

7.1 Principal Findings

7.1.1 Karst Hyporheic Models with Flat Impervious Ceiling

The first model of karst hyporheic flow that we consider consists of a conduit with a flat, impervious ceiling and a porous matrix floor. This morphology was chosen to isolate the effect of the floor morphology, a series of scallops (Figure 8). The modeled flow-field velocities and pressures, and resulting hyporheic zone, are depicted in Figure 9a & b. The graphics in this report contain colored contour plots presented without quantitative legends; the emphasis is on patterns and relative magnitude for explanatory understanding and not on quantitative values which might be inappropriately used for predictive purposes. As shown in the figure

the conduit has a velocity profile close to that of a parabola. The conduit fluid velocity slows at the upper and lower boundaries (no slip) and is a maximum in the center, not unlike that expected for a conduit with straight walls. In the absence of scallops, equipotential lines (lines of constant pressure) in the conduit would be parallel, and vertical. Since streamlines are always perpendicular to equipotential lines, flow would be horizontal. At the top of the conduit, where there are no scallops, the roughly parallel, vertical equipotential lines at the top of the conduit (Figure 9a) give rise to approximately horizontal flow in the same region (Figure 9b). Overall the scallops do not have a great influence on the net flow in the conduit, but they significantly change flow and fluid pressures near the scalloped wall (Figure 9a, b, d). Nested equipotential lines, which originate at the scallop peak, can be seen on the upstream and downstream side of each scallop (Figure 9a). The upstream equipotential lines signify a high pressure zone in front of the scallop, whereas the equipotential lines downstream to the scallop indicate a low pressure zone. In this low pressure zone eddies form just downstream of each scallop on their lee side (Figure 9b, c). The local pressure is highest near the point where the eddies reattach to the wall and lowest near the trough (lowest point) of the scallop. Much of the conduit water that enters the wall near the high pressure zone moves downstream through the matrix under the scallop's peak, eventually discharging back to the conduit at the low pressure zone on the lee side of the scallop. Some water entering the wall near the high pressure zone reverses direction and, like the adjacent eddy in the conduit, moves upstream in the matrix and discharges to conduit near the upstream trough.

In the matrix there is a point below the conduit wall and about half way between scallop peaks where equipotential lines of the same value converge, Figure 9a. At this point the flow rate drops to near zero and the flow direction converges; it is a stagnation point. These stagnation points indicate the dividing streamline between the hyporheic flow above and the ambient, lateral matrix flow below, as shown by the dark line in Figure 9b. Flow does not

cross this streamline: its depth defines the extent of the hyporheic zone. In this simulation the dividing streamline is located at the same depth below each scallop because the modeled scallops are of uniform size, spacing, and shape. The depth is maximum beneath the scallop's peak and about two-thirds as deep at its shallowest, halfway between adjacent peaks. The depth of this dividing streamline, and the hyporheic zone, depends on the conduit diameter; the flow rate; and the size, spacing, and shape of the scallops (and, as we will see later in other simulations the morphology of the ceiling).

If the conduit flow rate changes, the maximum depth of hyporheic flow in the matrix also changes, as demonstrated in Figure 9c. As the Reynolds number increases, the dividing streamline and penetration depth become deeper and more symmetric. The change in flow regime causes hyporheic flow to either move into "new" regions of the matrix or to retreat from regions of the matrix. In this way, as conduit flow rate changes over time, hyporheic flow might activate and deactivate reservoirs in the matrix that hold contamination, nutrients, or other solutes, as illustrated in Figure 6. Note that the stagnation point, the area of the matrix with the longest residence time (and a zero flow rate), moves with the dividing streamline and is therefore activated and deactivated, along with other areas of the matrix, with changing flow regime. The maximum depth of hyporheic flow changes more rapidly for lower conduit Reynolds numbers than for higher conduit Reynolds numbers (Figure 10).

One may infer from the asymptotic behavior of the curve in Figure 10 that there is a maximum depth of hyporheic flow for conduit Reynolds numbers above ~3,000. However, the flow for Reynolds numbers above ~2,500 requires a fully turbulent model, not the laminar flow mathematics used to produce the models represented by Figure 10. Because of the non-linearity inherent in turbulent flow, we do not believe that that asymptote shown in the figure is accurate for high Reynolds numbers. However, turbulent modeling studies of fluvial bedforms and stream hyporheic studies suggest that there will be an asymptote, just at a

different depth (Cardenas and Wilson, 2007a).

The ambient pressure gradient used to drive the flow in these simulations is very small due to the need for the simulations to remain non-turbulent and the large diameter of the conduit (see Figure 9 caption). Consequently, the simulated pressure gradients created in the matrix, and the conduit and matrix fluid velocities, are also small. However, the results presented in Figure 9 scale to any conduit size and pressure gradient, as they are reported in terms of Reynolds numbers. That is, they apply equally well to a 10 cm diameter conduit (1/10th the diameter) with geometric similitude, in which the scallops are also 1/10th the size. Low Reynolds number flows are more likely in smaller conduits.

7.1.2 Residence Time Distributions

The presence of hyporheic flow is not enough to prove its significance. The residence time of the hyporheic flow can help indicate what other processes it may affect, for example biogeochemical reactions (Gomez et al., 2012). If the residence time is extremely short and the hyporheic flow is fast, large volumes of water can sweep through the hyporheic zone but biogeochemical reactions along the flow path will be kinetically limited. If the residence time is extremely long and the flow is slow, then reactions can significantly change the water chemistry along the hyporheic flow path, but only small volumes of water will be exchanged with the conduit. Between these limits, conditions lead to the most important impacts where the volume of exchanged water is significant, and at least some reactions have enough time to take place.

Consider water age along hyporheic flow paths for a conduit with a flat, impervious ceiling, a porous matrix floor, a scallop floor morphology, and the flow field previously shown in Figure 9. The age is computed using COMSOL's non-reactive porous media solute-transport

capability and is shown in Figure 11b. Age increases with depth into the matrix and along hyporheic flow paths. The youngest water is found near the scallop peak where the flow paths are shortest and velocities are highest (Figure 11a). The spatial distribution of residence time for hyporheic water leaving the matrix is shown in Figure 11c. Residence times can be very short, for flow through the upper part of the scallop, to very long, for flow along the longest flow path, that is the one that approaches the deepest portion of the hyporheic zone. Even in a system with a maximum residence time of a year, other flow paths have residence times of days, weeks, or months, providing a wide variety of conditions for reactive biogeochemistry for DOC, nutrients, and contaminants. If the flow paths are too long the hyporheic water will be depleted of reactive components, too short and the kinetics may be too fast. Because of the variety of flow-path residence times in the system some of these flow paths will have just the right residence time (neither too long nor too short) to provide the correct conditions for reactive biogeochemistry.

The actual age values depend on the matrix permeability, matrix porosity, and the pressure distribution along the wall. Because the ambient pressure gradient used to drive the flow in these simulations is very small, the actual matrix velocities are also small and the longest residence times are very large (residence time does not approach infinity at zero velocity because of diffusion, and numerical dispersion). For a matrix permeability, k, of $10^{-11}\,\mathrm{m}^2$ and porosity of $\theta = 0.3$, the residence time along the longest flow path in Figure 9b is years. It is better to contrast the largest matrix residence time by comparing it to the residence time in the conduit, say, for the mean conduit flow over a distance of 1m, the distance between scallop peaks. With the same permeability and porosity given above, the longest matrix residence time in Figure 11c is eight million times longer than in the conduit (while the shortest matrix residence time is still effectively zero). Using that ratio, we can roughly extrapolate for the condition of turbulent flow in the conduit. If we assume a strong conduit mean velocity of

1m/s, the longest matrix hyporheic zone residence time would be three months.

7.1.3 Radial Symmetry and the Importance of Three-Dimensional Models

To explore the impact of ceiling and wall topography on the flow field, three models were constructed: a model with a flat impermeable ceiling, Figure 12a (this model is the same as shown in Figure 9), one with a contoured impermeable ceiling, Figure 12b, and a radially symmetric model with permeable walls on all sides, Figure 12c. The modeled scallops on the floor and ceiling in Figure 12b & c are symmetric. For all three models, the scallop shape and dimensions are the same, as is the matrix porosity and permeability, and the pressure drop across the domain. The conduit flow rate differs with different geometries (Reynolds number of 246, 142, 77 for Figure 12a, b, c respectively). For Figure 12b the maximum depth of hyporheic flow in the matrix below is slightly less than in Figure 12a, reflecting the influence of the upper scallops (maximum depth 0.65 m, 0.61 m, 0.48 m for Figure 12a, b, c respectively). Making fully 3D models is computationally challenging. We can begin to compare the difference between the model shown in Figure 12b and a 3D model by using a 2D model with radial symmetry (Figure 12c & f), a computationally simple way to make a 3D model for a rotationally symmetric geometry. The radial symmetric model has a much shallower depth of maximum hyporheic flow, 21% shallower than Figure 12b, and 25% shallower than Figure 12a. This indicates that modeling a realistic 3D conduit geometry is necessary to describe accurately describe conduit hyporheic flow. Figure 12d shows the pressure variation at the conduit matrix boundary for each of the three geometries. The largest pressure difference across the scallops is shown for the geometry in Figure 12a, with the flat ceiling. The pressure difference for the scalloped ceiling in Figure 12b is only slightly smaller, while the pressure difference for the radially symmetric case, Figure 12c, is significantly less. A plot of ages at the conduit matrix boundary is shown in Figure 12e,

while the ages for the radially symmetric case are also shown in Figure 12g. Ages for the scallop-ceiling case are somewhat lower because of the influence of the ceiling, and ages for the radially symmetric case are significantly lower. Ages are youngest downstream of each scallop.

7.1.4 Karst Hyporheic Flow Model with Contoured Permeable Ceiling

Since conduits have permeable ceilings that are not flat, the previous models are artificial. In conduits with ceiling cupolas the morphology of the conduit ceiling is typically of a larger scale than the floor or wall morphology, so a second model was constructed with a porous-matrix ceiling with two large cupolas, Figure 13, which result in changes in conduit area. Cupolas such as these are often found in caves. The porous-matrix floor of this model has periodic scallops with an amplitude smaller than and a spatial frequency greater than the cupolas.

Because they are larger features that impact conduit area, the ceiling cupolas have strong influence on the velocity field in the conduit (Figure 13a), including driving large-scale eddies that fill the ceiling cupolas (Figure 13b). There also remain smaller eddies downstream of the scallops lining the floor. The large-scale conduit flow pattern at the ceiling drives hyporheic flow to different and deeper depths in the ceiling matrix, than do scallops for the floor matrix, and causes longer and deeper hyporheic flow paths to circulate between the cupolas (Figure 13b). The influence of the ceiling morphology does not end there, but extends across the conduit to the floor where the pressure distribution on the floor has a similar large scale sensitivity to the presence the ceiling cupolas. Not only does the floor-matrix hyporheic zone have the small scale circulation associated with the scallops, it also has a larger and deeper scale hyporheic zone associated with effects of the ceiling. This larger scale, floor-matrix hyporheic exchange mimics that in the ceiling, although it does not penetrate as deeply.

The spatial pattern of age in the matrix forms a kind of boundary layer of younger, hyporheic water surrounding the conduit, illustrated in Figure 13c. For the floor matrix, this layer of younger hyporheic water lies only a short distance beneath the floor, but for the ceiling matrix it reflects the ceiling's deeper hyporheic zone and pattern of flow. Along the ceiling, the age is youngest on the downstream side of each cupola and oldest on the upstream side. Older ages penetrate deeper into the matrix above the cupolas, although that is due in large part to the fact that the cupolas themselves penetrate into the matrix. The actual thickness of the age boundary along the ceiling is greatest just upstream of each cupola. Although the ceiling morphology appears to have a significant impact on hyporheic flow in the floor matrix (Figure 13b), its influence not clearly show up in the floor's spatial pattern of age (Figure 13c). This is mainly due to a choice of color contours used in the figure and the differences in ages modeled in floor and ceiling. In any event, where the age discharges back to the conduit we calculate the spatial distribution of hyporheic exchange residence time.

The spatial distribution of residence time for water returning to the conduit from the matrix is shown in Figure 13d. The return flow from the ceiling is in the upper part of the figure, while that from the floor is in the lower part. Because the ceiling hyporheic zone is much larger and deeper, the maximum residence time and spatial extent is greater than from the floor. The return flow is older and, when you account for the velocities shown in Figure 13a,b, there is more of it. Both the ceiling and the floor have a variety of contributing flow paths of different lengths leading to a wide range of residence times (Figure 13d). Recall that the ceiling morphology appears to also have a significant impact on hyporheic flow in the floor matrix (Figure 13b), which did not clearly show in the spatial pattern of age (Figure 13c). However, it does show up for the residence time at the floor, with residence times associated with deeper floor-matrix hyporheic return flows associated with ceiling morphology having older water and broader zones of this older return flow.

The large conduit eddies in the dome of the cupolas could play an important role in designing and interpreting tracer tests which will be used in future field investigations of karst hyporheic zones. The eddies separate on the leeward side of ceiling morphology, on the upstream side of the cupolas (Figure 13b). Much smaller eddies occur on the lee side of scallops (Figure 9a; Figure 13b). The effect of cupolas on conduit eddies is more pronounced because they are wider and deeper than scallops, and because of their shape. Water can be trapped for a considerable length of time in the cupola eddies, leading to so-called long tails of tracer concentrations when observed in the conduit, as hypothesized by Wilson and Skiles (1988). When analyzing a tracer test for indication of hyporheic flow, it will be important to take into consideration the possibility of long residence time flow paths occurring in the conduit by mechanisms such as these cupola swirls. The best method to observe hyporheic flow via tracer test may be to sample water from inside the matrix immediately adjacent to the conduit wall.

7.2 Conclusions

The simulations of coupled conduit and matrix flow demonstrate that karst-conduit hyporheic flow is generated in the matrix located adjacent to a conduit, and is caused by conduit pressure fluctuations created by fluid flow over complex conduit-wall morphology and through the spatial variation of conduit cross-sectional area (scallops and cupolas) (see Figure 9b and Figure 13b). As conduit flow rate increases, the depth of hyporheic flow into the matrix also increases until it reaches an asymptote (Figure 9c and Figure 10). The spatial distribution of karst hyporheic flow residence time (Figure 11) always includes flow paths with residence times that are both long enough and short enough to suggest that hyporheic flow can, from the standpoint of reaction kinetics, play an important role in biogeochemical processes at the margin of karst conduits, likely influencing both natural chemistry and the sequestration and transformation of contaminants.

Models with 2D radially symmetry indicate that 2D Cartesian models models may be over-estimating the depth of the hyporheic flow by 21 - 25%. Radially symmetric models do not have a realistic conduit ceiling or wall geometry. Simulations with a permeable ceiling containing cupolas (Figure 13) showed that ceiling morphology significantly impacts hyporheic flow in the floor. Likewise, large scale floor matrix morphology would impact hyporheic flow in the ceiling matrix. The permeable ceiling models show the importance of using 3D models of hyporheic flow in future work. They also demonstrate a significant difference between hyporheic flow for karst conduits and fluvial streams since streams do not have ceilings. Future modeling should focus on 3D models with realistic conduit geometries, as well as accommodating the effects of turbulent flow in the conduit.

7.3 Recommendations to Water Resource Problems

Hyporheic flow is a well established concept for fluvial streams. Presented in this document is anecdotal evidence and model results that indicate hyporheic flow can be an important process in the matrix rock at the margin of karst phreatic conduits. Although our models focused on phreatic conduits (under the water table caves), the results are directly applicable to (vadose) cave streams and surface bedrock streams underlain by permeable rock.

When working in karst areas, water resource scientists should not assume that once water leaves the matrix and enters the conduit, it only exits from the conduit at a spring. This document indicates that conduit-matrix water exchanges occur wherever a mechanism creates a small scale pressure gradient (see Figure 5). These pressure gradients give rise to a hyporheic flow in the matrix, with a variety of residence time distributions and associated biogeochemical reactions.

Water resource managers and other decision makers should encourage field efforts to observe

karst hyporheic flow and its effects, and to assess its importance in speleogenesis, the evolution of natural water chemistry, and the sequestration and transformation of contaminants.

8 Summary

In fluvial systems the hyporheic zone is the subsurface volume where water enters from the stream, travels through the subsurface, and returns to the stream. It is a mixing zone between stream and aquifer waters that changes dynamically over space and time and is due to small-scale pressure variations in the stream channel caused by channel geometry and roughness, changes in channel area and conduit flow regime, and spatial and temporal variation of other properties and forcings. The fundamental fluid dynamics of karst conduits are not different from streams, with the Navier-Stokes equations describing flow in the conduit and Darcian flow in the sediment and rock-matrix porous media. Karst conduits have the same features that cause hyporheic flow in fluvial systems. Karst-conduit hyporheic exchange, and related biogeochemical processing, then becomes a fundamental component of the karst water cycle.

This report documents computational fluid dynamics simulations of karst hyporheic exchange developed using the finite element method. Laminar flow fields were generated for simulated phreatic karst conduits with no net exchange and conduit wall morphology. The flow field in the matrix was generated from the pressure distribution created at the conduit-wall boundary. COMSOL was used to produce 2D and axis-symmetric, steady-state models with realistic geometries and physical properties. The model simulations demonstrate karst hyporheic flow in the floor, ceiling, and side walls of matrix rock adjacent to karst conduits. The depth of hyporheic flow increases with the flow rate in the conduit and the size, spacing, and shape of the floor, ceiling, and side-wall morphological features. Ceiling morphology affects hyporheic

flow in the floor of the conduit, from across the diameter of the conduit, and vice versa, adding additional scaling of hyporheic flow not seen in fluvial systems. Modeling of the residence time of hyporheic flow shows a range of timescales indicating the flow can be important for a variety of biogeochemical processes, as well as contaminant sequestration and transformation.

9 References

Atkinson, T. C. (1977). Diffuse flow and conduit flow in limestone terrain in the Mendip Hills, Somerset (Great Britain). *Journal of Hydrology*, 35:93–110.

Bailly-Comte, V., Martin, J., Jourde, H., Screaton, E., Pistre, S., and Langston, A. (2010). Water exchange and pressure transfer between conduits and matrix and their influence on hydrodynamics of two karst aquifers with sinking streams. *Journal of Hydrology*, 386(1-4):55–66.

Bear, J. (1979). *Hydraulics of Groundwater*. Dover Publications Inc.

Beckie, R. (2005). Fundamental Hydrologic Equations. In Anderson, M. G., McDonnell, J. J., Bloeschl, G., and Sivapalan, M., editors, *Encyclopedia of Hydrological Sciences*, pages 1 – 16. John Wiley & Sons, Ltd.

Behrendt, H. (1996). Inventories of point and diffuse sources and estimated nutrient loads – A comparison for different river basins in central Europe. *Water Science and Technology*, 33:99–107.

Bencala, K. E. (1993). A perspective on stream-catchment connections. *Journal of the North American Benthological Society*, 12(1):44–47.

Bencala, K. E. (2011). Stream–Groundwater Interactions. In Wilderer, P., editor, *Treatise on Water Science*, pages 537–546. Oxford Academic Press.

Bethke, C. and Johnson, T. (2002). Paradox of groundwater age: Correction. *Geology*, 30(4):385–388.

Bethke, C. M. and Johnson, T. M. (2008). Groundwater age and groundwater age dating. *Annual Review of Earth and Planetary Sciences*, 36:121–152.

Blumberg, P. N. and Curl, R. L. (1974). Experimental and theoretical studies of dissolution roughness. *Journal of Fluid Mechanics*, 65:735 –751.

Boulton, A. J., Findlay, S., Marmonier, P., Stanley, E. H., and Valett, H. M. (1998). The functional significance of the hyporheic zone in streams and rivers. *Annual Review of Ecology and Systematics*, 29:59–81.

Budd, D. A. and Vacher, H. L. (2004). Matrix permeability of the confined Floridan Aquifer, Florida, USA. *Hydrogeology Journal*, 12(5):531–549.

Buffington, J. M. and Tonina, D. (2009). Hyporheic exchange in mountain rivers ii: Effects of channel morphology on mechanics, scales, and rates of exchange. *Geography Compass*, 3(3):1038–1062.

Cardenas, M. B. (2009). Stream-aquifer interactions and hyporheic exchange in gaining and losing sinuous streams. *Water Resources Research*, 45:W06429.

Cardenas, M. B. and Gooseff, M. N. (2008). Comparison of hyporheic exchange under covered and uncovered channels based on linked surface and groundwater flow simulations. *Water Resources Research*, 44(3):W03418.

Cardenas, M. B. and Wilson, J. L. (2007a). Dunes, turbulent eddies, and interfacial exchange with permeable sediments. *Water Resources Research*, 43:W08412.

Cardenas, M. B. and Wilson, J. L. (2007b). Effects of current–bed form induced fluid flow on the thermal regime of sediments. *Water Resources Research*, 43:W08431.

Cardenas, M. B. and Wilson, J. L. (2007c). Exchange across a sediment-water interface with ambient groundwater discharge. *Journal of Hydrology*, 346:69–80.

Cardenas, M. B., Wilson, J. L., and Haggerty, R. (2008). Residence time of bedform-driven hyporheic exchange. *Advances in Water Resources*, 31(10):1382–1386.

Cardenas, M. B., Wilson, J. L., and Zlotnik, V. A. (2004). Impact of heterogeneity, bed forms, and stream curvature on subchannel hyporheic exchange. *Water Resources Research*, 40:W08307.

Chu, Y. and Gelhar, L. (1972). Turbulent pipe flow with granular permeable boundaries. Technical report, Ralph M. Parsons Laboratory for Water Resources & Hydrodynamics, Report No: 148, Massachusetts Institute of Technology, Cambridge, Mass.

Courant, R. (1943). Variational methods for the solution of problems of equilibrium and vibrations. *Bulletin of the American Mathematical Society*, 49:1–23.

Dahm, C., Valett, H. M., Baxter, C. V., and Woessner, W. W. (2006). Hyporheic zones. In Hauer, F. and Lamberti, G., editors, *Methods in Stream Ecology*, pages 119–142. Academic Press, Inc., San Diego, CA.

Darcy, H. (1856). *Les fontaines publiques de la ville de Dijon.* Libraire des Corps Imperiaux des Ponts et Chaussées et des Mines, Paris.

de Montety, V., Martin, J. B., Cohen, M. J., Foster, C., and Kurz, M. J. (2011). Influence of diel biogeochemical cycles on carbonate equilibrium in a karst river. *Chemical Geology*, 283(1-2, Sp. Iss. SI):31–43.

Dodds, W. K. and Cole, J. J. (2007). Expanding the concept of trophic state in aquatic ecosystems: It's not just the autotrophs. *Aquatic Sciences*, 69:427 – 439.

Dogwiler, T. and Wicks, C. (2005). Thermal variations in the hyporheic zone of a karst stream. *Speleogenesis and Evolution of Karst Aquifers*, 3(2).

Elliott, A. H. and Brooks, N. H. (1997). Transfer of nonsorbing solutes to a streambed with bed forms: Theory. *Water Resources Research*, 33(1):123–136.

Engdahl, N. B., Vogler, E. T., and Weissmann, G. S. (2010). Evaluation of aquifer heterogeneity effects on river flow loss using a transition probability framework. *Water Resources Research*, 46:W01506.

Faulkner, J., Hu, B. X., Kish, S., and Hua, F. (2009). Laboratory analog and numerical study of groundwater flow and solute transport in a karst aquifer with conduit and matrix domains. *Journal of Contaminant Hydrology*, 110:34–44.

Fiebig, D. M. (1995). Groundwater discharge and its contribution of dissolved organic carbon to an upland stream. *Archiv für Hydrobiologie*, 124:129–155.

Field, M. (1988). The vulnerability of karst aquifers to chemical contamination. In *Conference proceedings of the American Institute of Hydrology Conference, November 16-18*, Tampa, FL.

Field, M. (1993). Karst hydrology and chemical contamination. *Journal of Environmental Systems*, 22:1–16.

Fischer, H., Kloep, F., Wilzcek, S., and Pusch, M. T. (2005). A river's liver: microbial processes within the hyporheic zone of a large lowland river. *Biogeochemistry*, 76:349–371.

Fleckenstein, J. H., Niswonger, R. G., and Fogg, G. E. (2006). River-Aquifer Interactions, Geologic Heterogeneity, and Low-Flow Management. *Ground Water*, 44(6):837–852.

Florea, L. (2006). *The Karst of West-Central Florida*. PhD thesis, University of South Florida, Tampa, FL.

Ford, D. and Williams, P. (2007). *Karst Hydrogeology and Geomorphology*. John Wiley & Sons Ltd, West Sussex, England.

Fritz, B. G. and Arntzen, E. V. (2007). Effect of rapidly changing river stage on uranium flux through the hyporheic zone. *Ground Water*, 45(6):753–760.

Furbish, D. J. (1997). *Fluid Physics in Geology*. Oxford University Press.

Ginn, T. R. (1999). On the distribution of multicomponent mixtures over generalized exposure time in subsurface flow and reactive transport: Foundations, and formulations for groundwater age, chemical heterogeneity, and biodegradation. *Water Resources Research*, 35(5):1395–1407.

Goldscheider, N., Drew, D., and Worthington, S. (2007). Introduction. In Goldscheider, N. and Drew, D., editors, *Methods in Karst Hydrogeology*, volume 26 of *IAH: International Contributions to Hydrogeology*, chapter 1, pages 1–8. Taylor & Francis.

Gomez, J. D., Wilson, J. L., and Cardenas, M. B. (2012). Residence time distributions in sinuosity-driven hyporheic zones and their biogeochemical effects. *Water Resources Research*, 48:W09533.

Goode, D. J. (1996). Direct simulation of groundwater age. *Water Resources Research*, 32(2):289–296.

Gooseff, M. N. (2010). Defining hyporheic zones – advancing our conceptual and operational definitions of where stream water and groundwater meet. *Geography Compass*, 4(8):945–955.

Gu, C., Hornberger, G. M., Mills, A. L., Herman, J. S., and Flewelling, S. A. (2007). Nitrate reduction in streambed sediments: Effects of flow and biogeochemical kinetics. *Water Resources Research*, 43(12).

Haggerty, R., Marti, E., Argerich, A., von Schiller, D., and Grimm, N. B. (2009). Resazurin as a "smart" tracer for quantifying metabolically active transient storage in stream ecosystems. *Journal of Geophysical Research–Biogeosciences*, 114:G03014.

Hancock, P. J., Boulton, A. J., and Humphreys, W. F. (2005). Aquifers and hyporheic zones: Towards and ecological understanding of groundwater. *Hydrogeology Journal*, 13(1):98–111.

Hendricks, S. P. (1993). Microbial ecology of the hyporheic zone – a perspective integrating hydrology and biology. *Journal of the North American Benthological Society*, 12(1):70–78.

Henry, K. and Wilson, J. (2014). Karst-conduit hyporheic exchange. *Hydrology & Earth System Science*, in preparation.

Henry, K., Wilson, J., and Kincaid, T. (2011). Experimental design of a dye trace from conduit to matrix. *Geological Society of America Abstracts with Program*, 43(5):290.

Henry, K. and Wilson, J. L. (2011a). Karst hyporheic exchange below conduits with turbulent flow. *Eos Transactions, AGU, Fall Meeting Supplement*, pages H23F–1333.

Henry, K. and Wilson, J. L. (2011b). Residence times of karst conduit hyporheic flow. *Geological Society of America Abstracts with Program*, 43(5):341.

Ho, R. and Gelhar, L. (1973). Turbulent flow with wavy permeable boundaries. *Journal of Fluid Mechanics*, 58(2):403–414.

Ho, R. T. and Gelhar, L. W. (1974). Interaction between turbulent flow and undular permeable boundaries. Technical report, Ralph M. Parsons Laboratory for Water Resources & Hydrodynamics, Report No 180, Massachusetts Institute of Technology, Cambridge, Mass.

Ho, R. T. and Gelhar, L. W. (1983). Turbulent flow over undular permeable boundaries. *Journal of Hydraulic Engineering*, 109(5):741–756.

Katz, B. G., Chelette, A. R., and Pratt, T. R. (2004). Use of chemical and isotopic tracers to assess nitrate contamination and ground-water age, woodville karst plain, usa. *Journal of Hydrology*, 289:36–61.

Kazemi, G. A., Lehr, J. H., and Perrochet, P. (2006). *Groundwater Age*. John Wiley & Sons, Inc.

Kazezyilmaz-Alhan, C. M. (2008). Analytical solutions for contaminant transport in streams.

Journal of Hydrology, 348(3-4):524–534.

Landmeyer, J. E., Bradley, P. M., Trego, D. A., Hale, K. G., and Haas, II, J. E. (2010). MTBE, TBA, and TAME Attenuation in Diverse Hyporheic Zones. *Ground Water*, 48(1):30–41.

Li, G. (2004). *Laboratory simulation of solute transport and retention in karst*. PhD thesis, Florida State University.

Li, G., Loper, D. E., and Kung, R. (2008). Contaminant sequestration in karstic aquifers: Experiments and quantification. *Water Resources Research*, 44(2):22.

Loop, C. M. and White, W. B. (2001). A conceptual model for dnapl transport in karst ground water basins. *Ground Water*, 39(1):119–127.

Mahler, B. and Massie, N. (2007). Anthropogenic contaminants as tracers in an urbanizing karst aquifer. *Journal of Contaminant Hydrology*, 91(1–2):81–106.

Malcolm, I. A., Soulsby, C., Youngson, A. F., and Tetzlaff, D. (2009). Fine scale variability of hyporheic hydrochemistry in salmon spawning gravels with contrasting groundwater-surface water interactions. *Hydrogeology Journal*, 17(1):161–174.

Martin, J. and Dean, R. (2001). Exchange of water between conduits and matrix in the Floridan Aquifer. *Chemical Geology*, 179:145–165.

Moore, P., Martin, J., and Screaton, E. (2009). Geochemical and statistical evidence of recharge, mixing, and controls on spring discharge in an eogenetic karst aquifer. *Journal of Hydrology*, 376(3-4):443–455.

Mulholland, P. (1997). Evidence that hyporheic zones increase heterotrophic metabolism and phosphorous uptake in forest streams. *Limnology and Oceanography*, 42:443–451.

Munoz Goma, R. and Gelhar, L. (1968). Turbulent pipe flow with rough and porous walls. Technical report, Hydrodynamics Laboratory, Department of Civil Engineering, Report No 109, Massachusetts Institute of Technology, Cambridge, Mass.

Navier, C. L. M. H. (1822). Memoire sur les lois du mouvement des fluides. *Mémoires Académie royale des sciences de Paris*, 6:389–416.

Niswonger, R. G., Prudic, D. E., Fogg, G. E., Stonestrom, D. A., and Buckland, E. M. (2008). Method for estimating spatially variable seepage loss and hydraulic conductivity in intermittent and ephemeral streams. *Water Resources Research*, 44(5).

Olsen, R. and Eckhert, E. (1966). Experimental studies of turbulent flow in a porous circular tube with uniform fluid injection through the tube wall. *Transactions of the ASME*, 33:7–17.

Orghidan, T. (1955). Un nou domeniu de viata acvatica subterana 'biotopul hiporeic'. *Buletin Stiintific sectia de Biologie si stiinte Agricole si sectia de Geologie si Geografie [Romania – Academy of Sciences]*, 7(3):657–676.

Orghidan, T. (1959). Ein neuer Lebensraum des unterirdischen Wassers: der hyporheische

Biotop. *Archiv für Hydrobiologie*, 55:392–414.

Orghidan, T. (2010). A new habitat of subsurface waters: the hyporheic biotope. *Fundamental and Applied Limnology / Archiv für Hydrobiologie*, 176(4):291–302.

Palmer, A. (2007). *Cave Geology*. Cave Books, Huntsville, AL.

Paulson, R., Chase, E., Roberts, R., and Moody, D. (1990). National Water Summary 1988-89: Hydrologic Events and Floods and Droughts. Technical report, USGS Water Supply Paper Report No: 2375.

Pusch, M., Fiebig, D., Brettar, I., Eisenmann, H., Ellis, B. K., Kaplan, L. A., Lock, M. A., Naegeli, M. W., and Traunspurger, W. (1998). The role of micro-organisms in the ecological connectivity of running waters. *Freshwater Biology*, 40:453–496.

Ritorto, M. (2007). Impacts of diffuse recharge on transmissivity and water budget calculations in the unconfined karst aquifer of the Santa Fe River basin. Master's thesis, University of Florida.

Rotenberg, M. (1972). Theory of population transport. *Journal of Theoretical Biology*, 37:291–305.

Salehin, M., Packman, A. I., and Paradis, M. (2004). Hyporheic exchange with heterogeneous streambeds: Laboratory experiments and modeling. *Water Resources Research*, 40(11):18.

Simon, K. and Benfield, E. (2002). Ammonium retention and whole-stream metabolism in cave streams. *Hydrobiologia*, 482(1):31–39.

Smith, J. (2005). Groundwater-surface water interactions in the hyporheic zone. Technical report, Environmental Agency, Bristol, UK.

Sophocleous, M. (2002). Interactions between groundwater and surface water: the state of the science. *Hydrogeology Journal*, 10(1):52–67.

Stokes, G. G. (1845). On the theories of the internal friction of fluids in motion, and of the equilibrium and motion of elastic solids. *Transactions of the Cambridge Philosophical Society*, 8:287–305.

Streeter, V. and Wylie, E. (1983). *Fluid Mechanics*. McGrawHill, New York, NY.

Tonina, D. and Buffington, J. (2009). Hyporheic exchange in mountain rivers i: Mechanics and environmental effects. *Geography Compass*, 3(3):1063–1086.

Triska, F. J., Kennedy, V., Avanzino, R. J., Zellweger, G., and Bencala, K. (1989). Retention and transport of nutrients in a third-order stream in northwest California: hyporheic processes. *Ecology*, 79(6):1893–1905.

Vesper, D. (2008). Karst resources and other applied issues. In Martin, J. and White, W., editors, *Frontiers of Karst Research*, volume 13, pages 65–73, Leesburg, VA. Karst Waters Institute.

Vesper, D. and Schindel, G. (2008). Focus group on karst resources and other applied issues.

In Martin, J. and White, W., editors, *Frontiers of Karst Research*, volume 13, pages 106–107, Leesburg, VA. Karst Waters Institute.

Vesper, D. and White, W. (2006). Comparative storm response of contaminants in a carbonate aquifer, Fort Campbell, Kentucky-Tennessee. In Harmon, R. and Wicks, C., editors, *Perspectives on Karst Geomorphology, Hydrology and Geochemisry*, number 404 in Special Paper, pages 267–274, Boulder, Colorado. The Geological Society of America.

White, D. S. (1993). Perspectives on defining and delineating hyporheic zones. *Journal of the North American Benthological Society*, 12:61–69.

White, W. (1999). Conceptual models for karstic aquifers. In Palmer, A., Palmer, M., and Sasowsky, I., editors, *Karst Modeling*, pages 11–16. Karst Waters Institute, Charlestown, WV.

White, W. (2002). Karst hydrology: recent developments and open questions. *Engineering Geology*, 65:85–105.

White, W. and White, E. (2005). Ground water flux distribution between matrix, fractures, and conduits: constraints on modeling. *Speleogenesis and Evolution of Karst Aquifers*, 3:1–6.

White, W. B. (1988). *Geomorphology and Hydrology of Karst Terrains*. Oxford University Press, New York.

Wilson, J. and Henry, K. (2014). Matrix storage of phreatic karst flood waters. *Ground Water*, in preparation.

Wilson, W. and Skiles, W. (1988). Aquifer characterization by quantitative dye tracing at Ginnie Spring, northern Florida. In *Second Conference on Environmental Problems in Karst Terranes and Their Solutions*, pages 121–141. National Water Well Association, Dublin, OH.

Wohl, E. (2010a). *Mountain Rivers Revisited*, volume 19 of *Water Resources Monograph*. American Geophysical Union, Washington, DC.

Wohl, E. (2010b). Private communication. April 6.

Worthington, S. R. H., Ford, D. C., and Deddows, P. A. (2000). Porosity and permeability enhancement in unconfined carbonate aquifers as a result of solution. In Klimchouk, A. B., Ford, D. C., Palmer, A. N., and Dreybrodt, W., editors, *Speleogenesis: Evolution of Karst Aquifers*, chapter 8.1, pages 463–472. National Speleological Society, Huntsville, Alabama, USA.

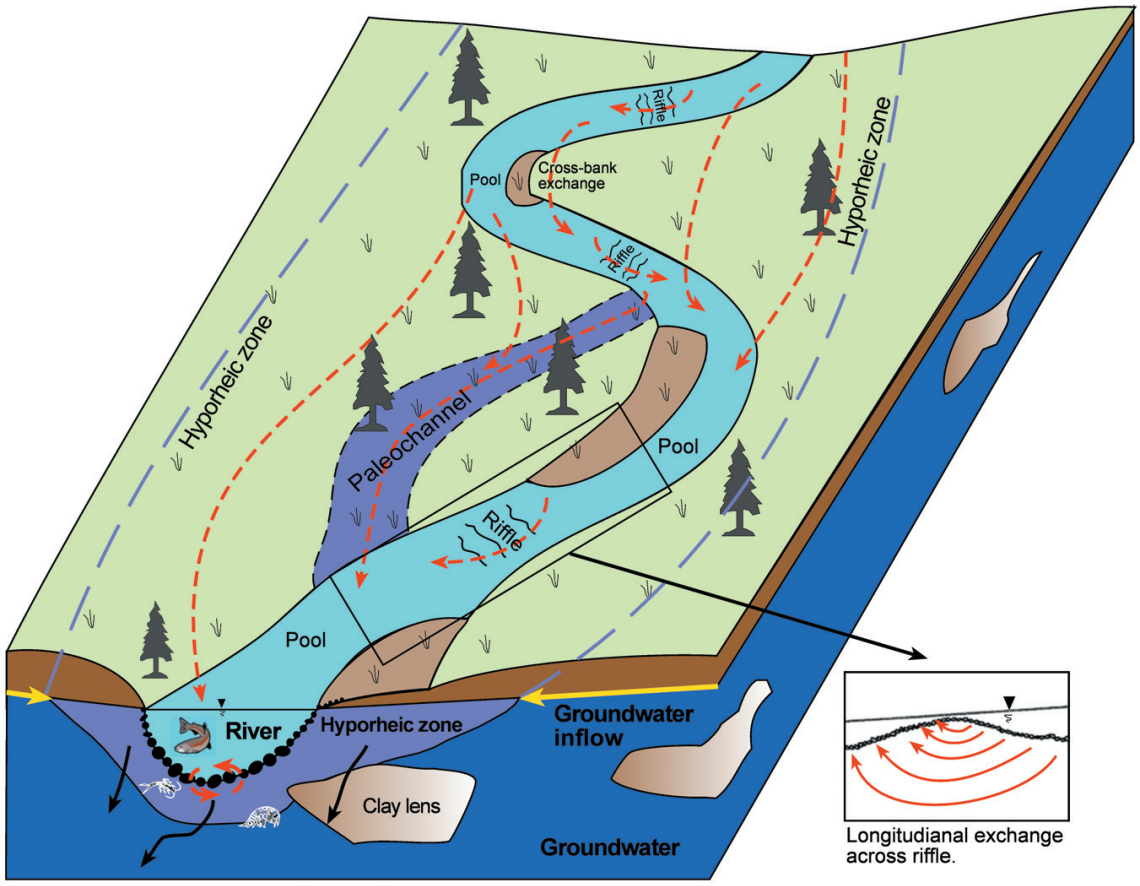

Figure 1: Hyporheic exchange in a stream. The hyporheic zone around a river is defined by the extent of surface-subsurface mixing surrounding a river. Different from hyporheic flow (red arrows) is far-field inflow of groundwater (solid yellow arrows) and one-way outflow of groundwater (black arrows). From Tonina and Buffington (2009).

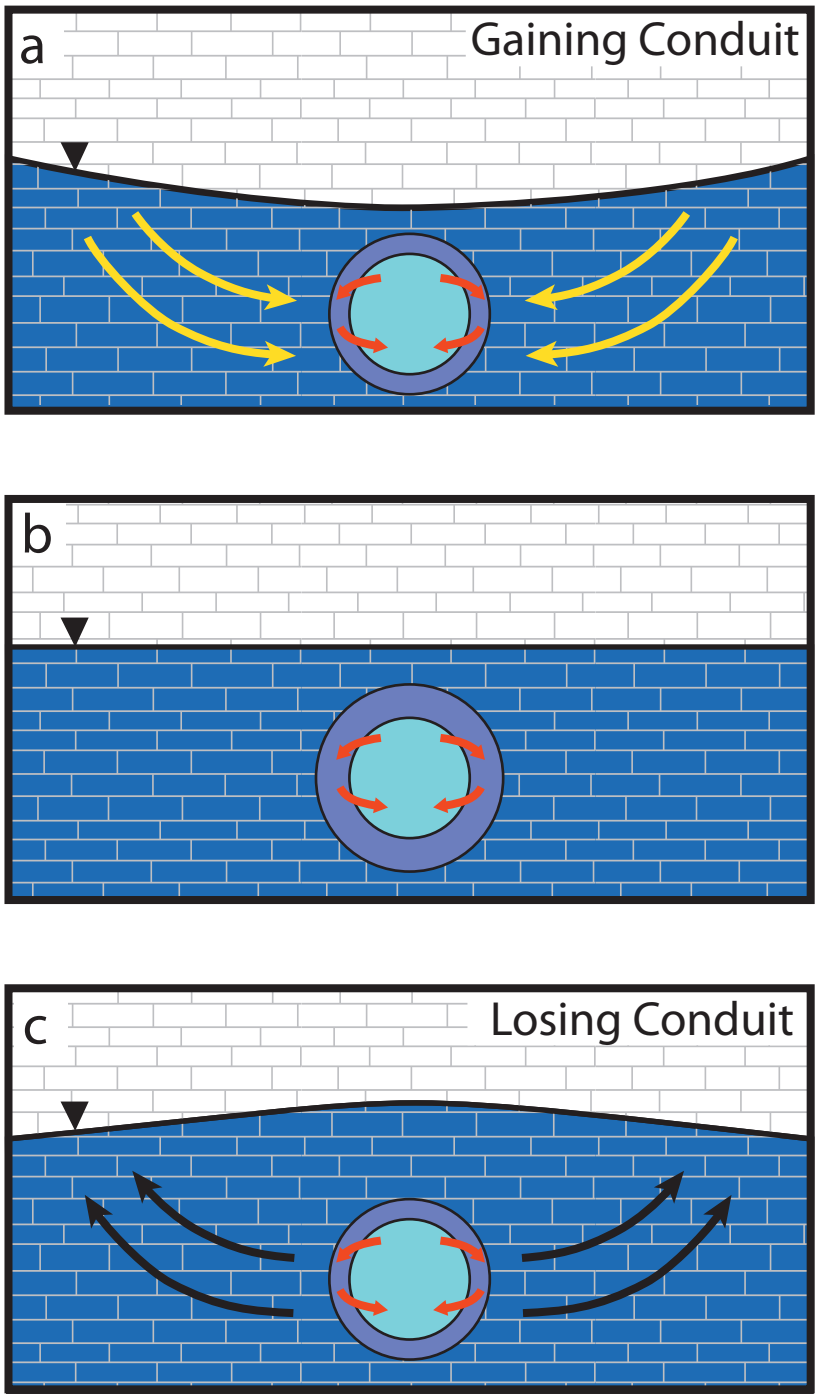

Figure 2: Cross-section of conduit-matrix exchanges in a karst aquifer. Color scheme is the same as Figure 1. Cases a and c representing gaining and losing conduits, respectively, while b represents a a conduit with no net loss or gain to the matrix. Influenced by White (1999).

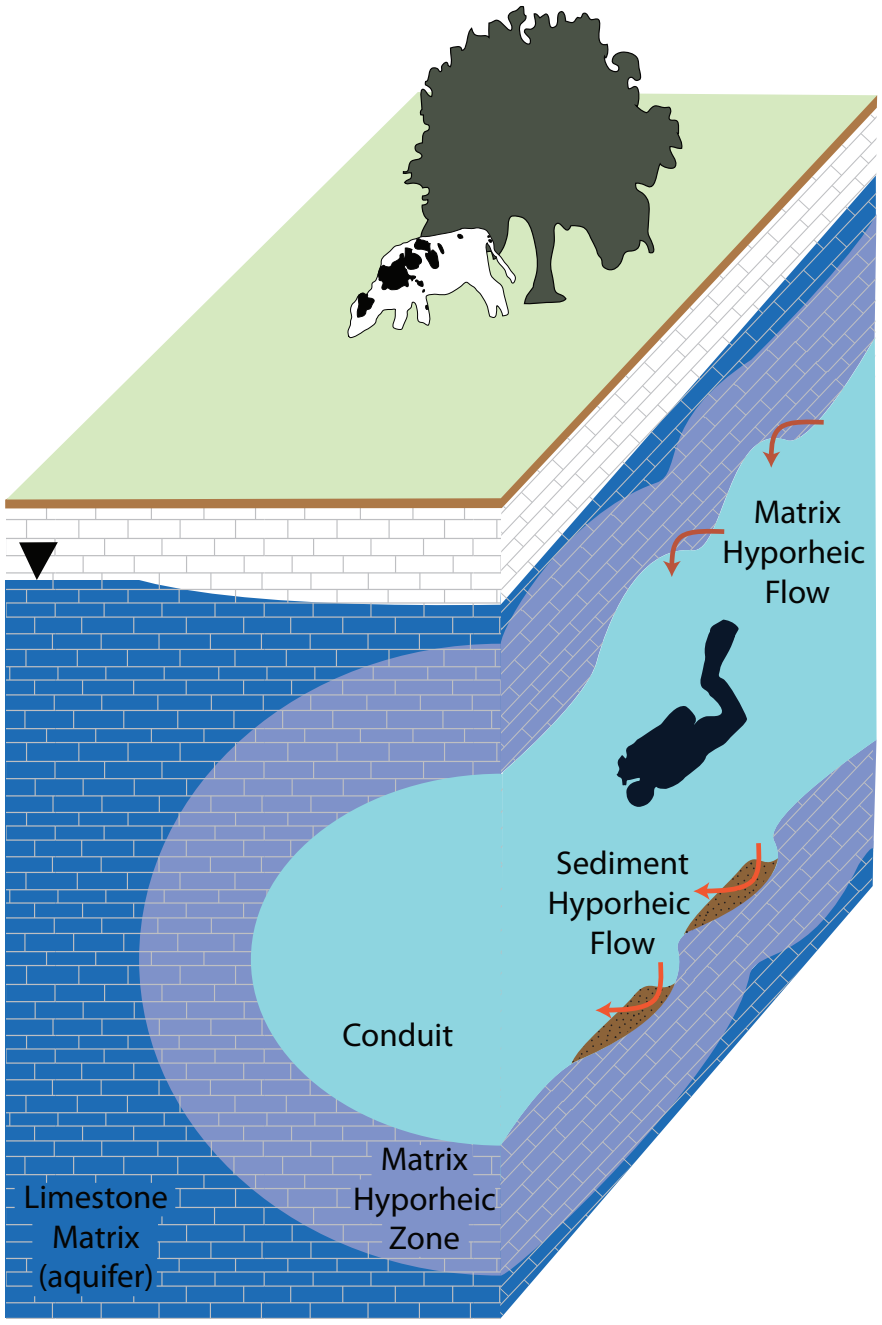

Figure 3: Cut-away of karst hyporheic flow in a karst aquifer. The 2D longitudinal section on the right is used for the 2D mathematical model presented later in this report. Color scheme is similar to Figure 1 but with dark orange arrows illustrating sediment hyporheic flow and light orange arrows illustrating matrix hyporheic flow.

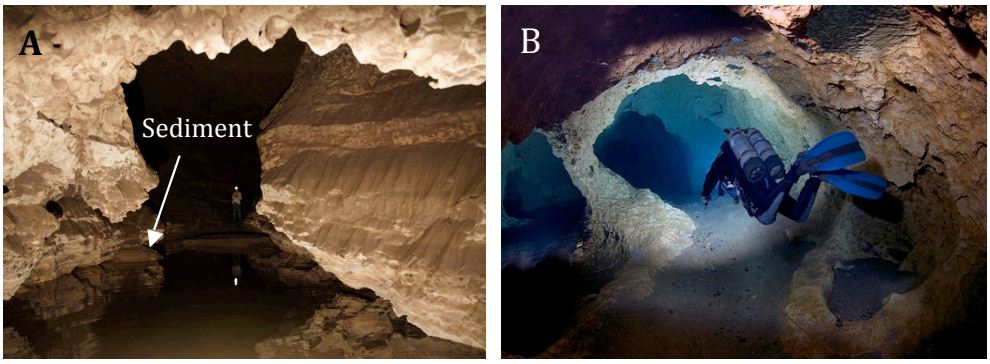

Figure 4: Environments typical of karst hyporheic flow. a: Typical vadose cave stream with sediment in the stream bed and along sides (Location: Crystal Creek at the Northern terminus of Snowy River in Ft. Stanton Cave, NM. Photograph reproduced with permission from James Hunter). b: Typical phreatic karst conduit with sediment. Notice the pocket of sediment on the lower right and the complex conduit wall morphology. (Location: Peacock Springs, FL. Photograph reproduced with permission from Jill Heinerth.)

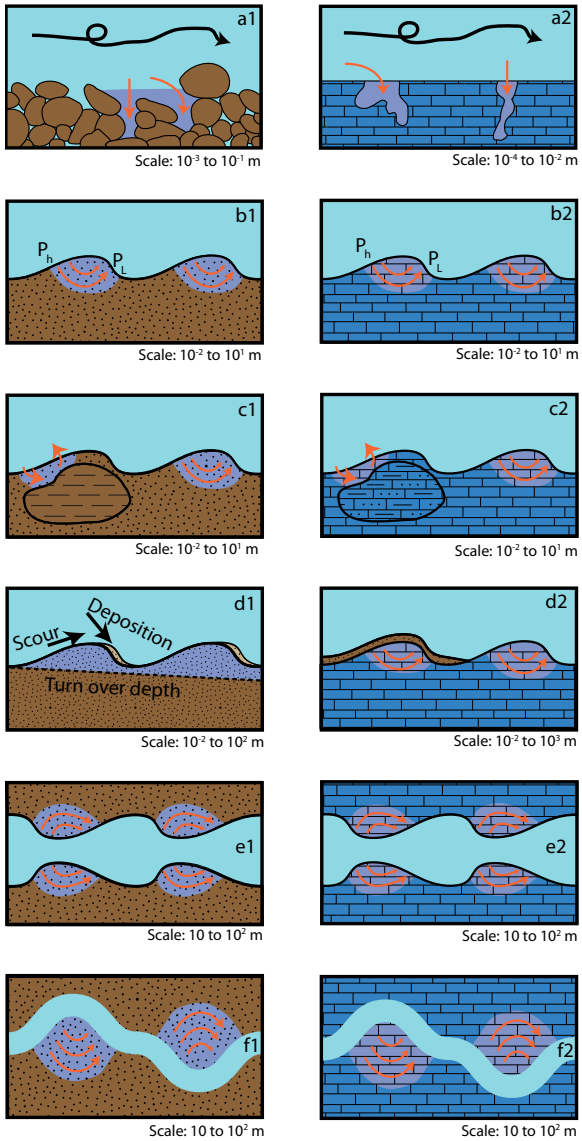

Figure 5: Some mechanisms of karst-conduit hyporheic exchange in sediment (left column) and rock (right column). Color scheme similar to Figure 1. Each mechanism causes a small scale pressure gradient that gives rise to hyporheic exchange. Mechanisms: side view: (a) turbulence at conduit-sediment (left) or conduit-matrix (right) interface (analogous to fluvial near-bed turbulence) (b) spatial variation in pressure at conduit-sediment (left) or conduit-matrix (right) pressure head (analogous to near-bed pressure head variation in a fluvial system); (c) spatial variation in hydraulic conductivity; (d) sediment bedload transport; top view: (e) spatial variation in channel/conduit area (f) sinuosity. All of the rock exchanges can occur under a thin layer of sediment (such as shown in d2). Although only the bottom or sides of the conduit is shown, these could occur where ever there is sediment or rock in the conduit. Influenced by Tonina and Buffington (2009).

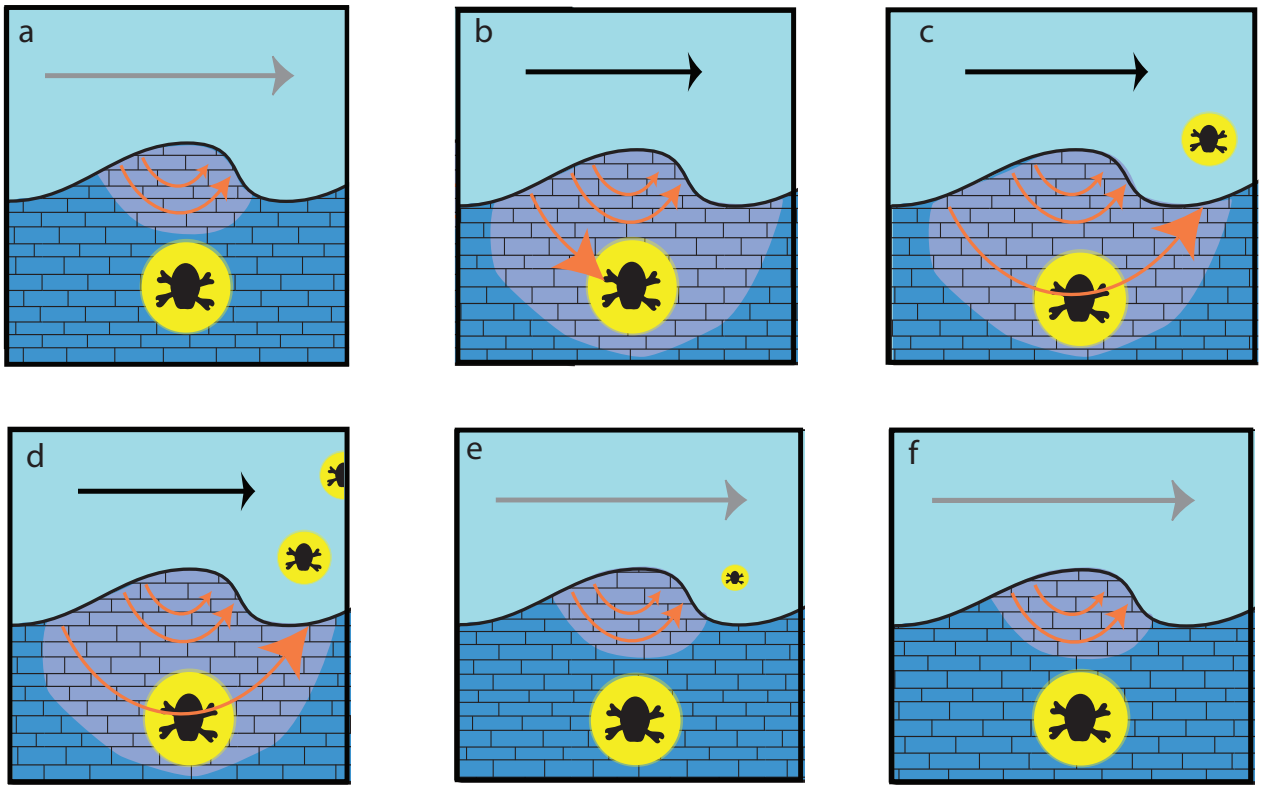

Figure 6: Example of matrix contaminant mobilization with changing conduit flow regime a) Initial state with contaminant reservoir sequestered in matrix, and not mobilized by hyporheic flow. b) Flow regime changes in conduit, hyporheic flow extends and reaches contamination. c) Some of the contamination is mobilized and advected to conduit by hyporheic flow. d) Contamination concentration increases in conduit. e) Flow regime returns to initial state, some contamination still present in conduit. f) Concentrations in conduit return to initial state with sequestered contaminant reservoir still in matrix.

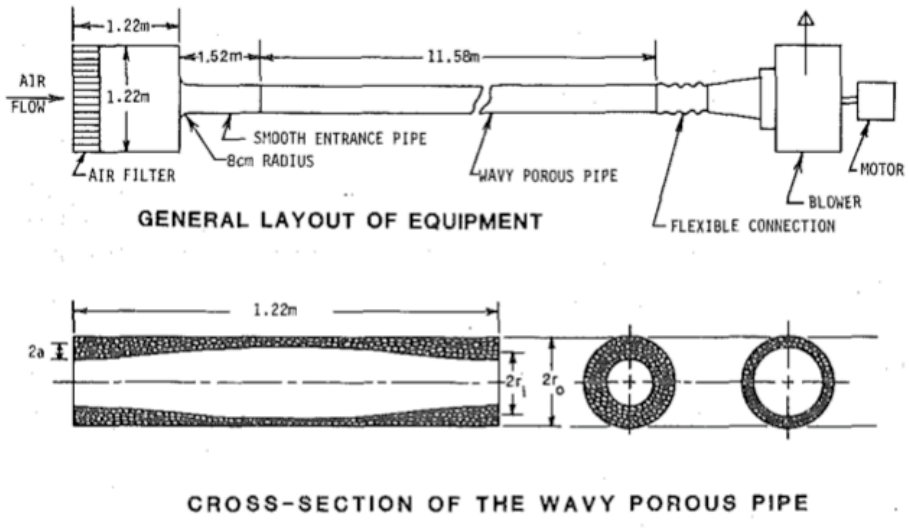

Figure 7: Experimental design of MIT laboratory experiment. Top: General design; bottom: one section of the wavy porous pipe. From Ho and Gelhar (1983).

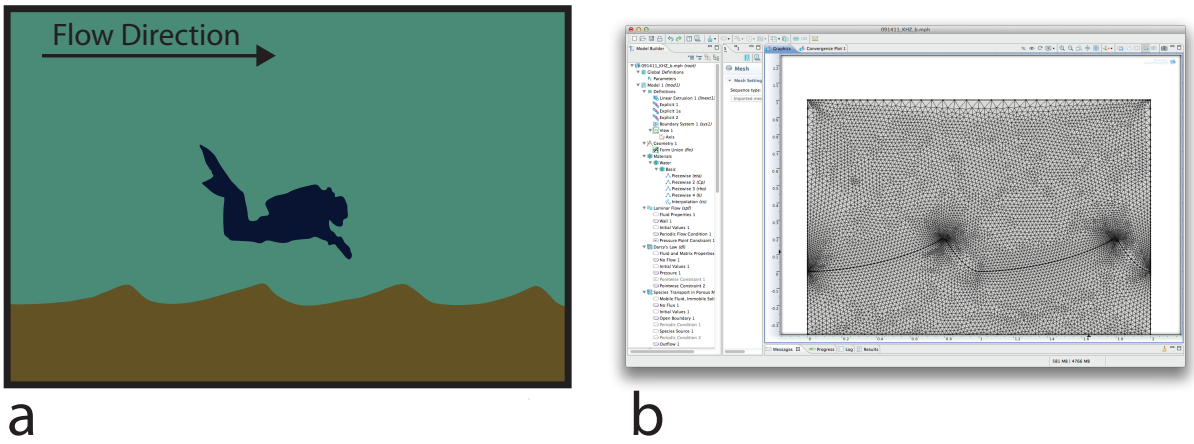

Figure 8: a) Typical physical 2D cross section through a conduit and matrix, with ceiling at the top and floor at the bottom, and b) typical model domain. Depicted is a conduit with flat impervious ceiling and scallop lined porous matrix floor.

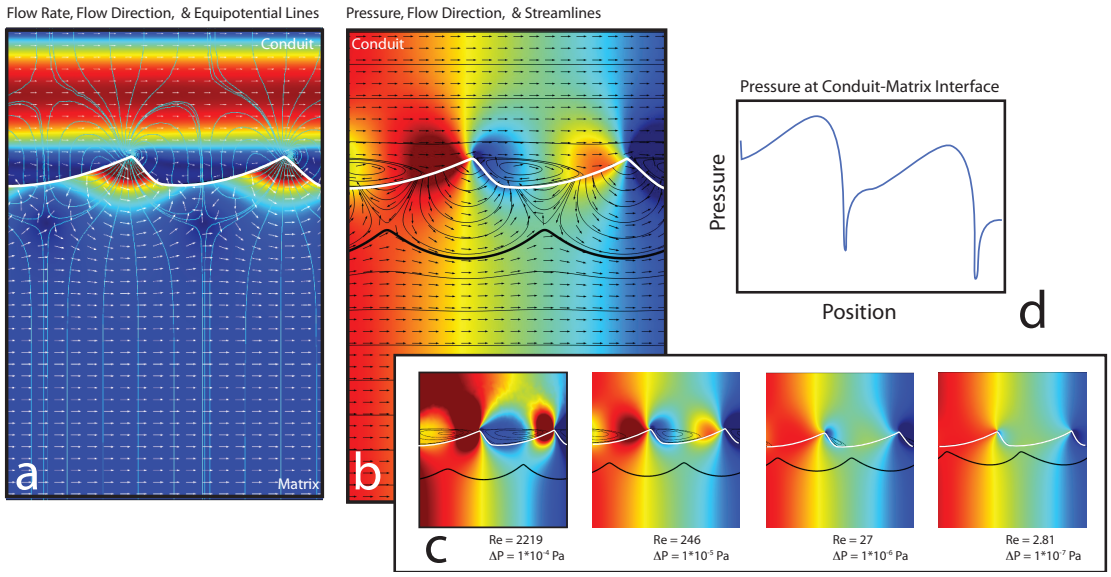

Figure 9: Model of karst hyporheic flow through the matrix underlying a conduit, with a flat, impervious ceiling at the top and regularly spaced, scalloped conduit wall and matrix at the bottom. a) Flow rate, flow direction, & equipotential lines. Color is flow rate (red = high, blue = low). Arrows show flow direction. Lines of equal pressure are shown in light blue. Velocity distribution is close to parabolic in the conduit, and greatest in the matrix immediately below the scallop peaks. Flowpaths, shown by streamlines in b, are always perpendicular to equipotential lines. $\Delta p = 10^{-5}$ Pa; Re = 246. b) Pressure distribution & flow field. Color is pressure (red = high, blue = low). Arrows show flow direction. Flow paths are shown for the conduit, illustrating the eddy downstream of the scallop peak, and matrix, illustrating the hyporheic zone with its maximum depth shown by a thicker flow line. $\Delta p = 10^{-5}$ Pa; Re = 246. c) Results of hyporheic flow for a range of conduit Reynolds numbers, $\mathbf{Re} = \overline{u}_x b/\nu$, where $\overline{u}_x$ is the mean longitudinal velocity in the conduit and b is its diameter. The depth of hyporheic flow in the matrix increases as flow velocity increases in the conduit. The eddie size in the conduit also increases with flow velocity in the conduit. d) Pressure at conduit-matrix boundary (the conduit wall) for model shown in a & b. Pressure at conduit wall is calculated by solving the Navier-Stokes equations in the conduit and is prescribed as a boundary condition on the matrix. Parameters: conduit diameter (measured from scallop trough) = b = 1 m; scallop wave length (distance between peaks) = λ = 1 m; scallop height = H = 0.2 m; total matrix depth beneath the floor = 2 m; length of domain = 2λ = 2 m; temperature = 20°C (determines water density and viscosity). Flow direction and pressure results in this figure do not change with matrix permeability, k, or porosity, θ.

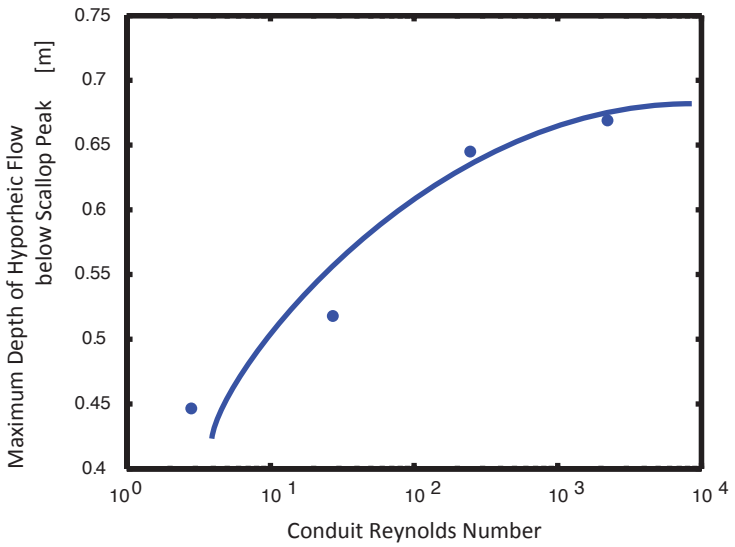

Figure 10: Maximum depth of hyporheic flow below top of scallop as a function of conduit Reynolds number, $\mathbf{Re} = \overline{u}_x b/\nu$, for the conditions depicted in Fig. 9a. Recall that the total matrix depth beneath the floor = 2 m, about three times as large as the asymptote. Plot valid only for a laminar flow regime in the conduit and should not be extrapolated to turbulent flow.

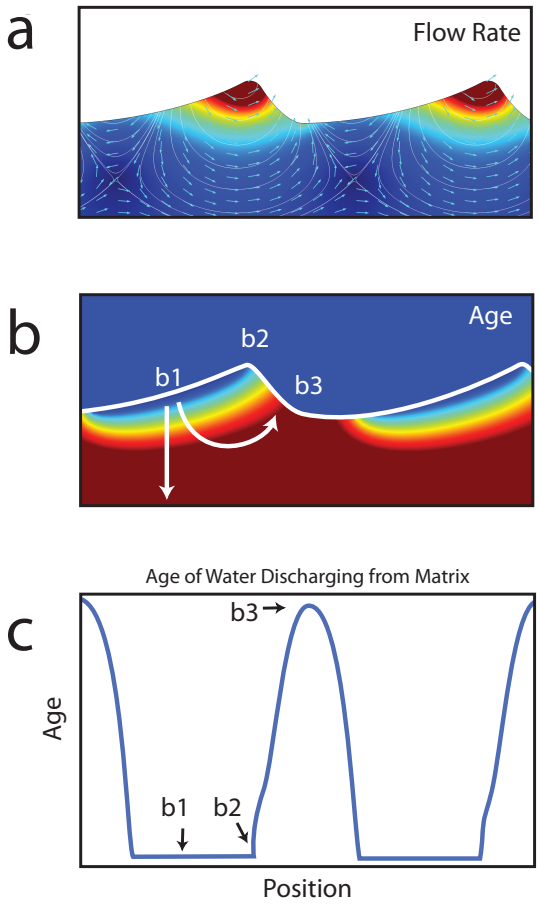

Figure 11: Relative ages and residence times of karst hyporheic zone in the matrix for the conditions depicted in Figure 9a. a) Velocities of hyporheic flow. Color is relative speed (red= fast, blue = slow). b) Age of hyporheic flow. Color is relative age (red= old, blue = new). c) Spatial distribution of relative residence time in water returning to the conduit. Actual speed, age and residence time depend on k and θ values. Notice that at b1) age increases with depth into hyporheic zone; b2) age is youngest at high point of the scallop; b3) age increases along flow path; and b2 to b3) age changes from zero to a maximum along the portion of floor where the hyporheic zone discharges back to the conduit. In c) the zero values represent areas, like location b1, where water is entering the matrix from the conduit. Parameters: conduit diameter (measured from scallop trough) = $b = 1\,\mathrm{m}$; scallop wave length (distance between peaks) = $\lambda = 1\,\mathrm{m}$; scallop height = $H = 0.2\,\mathrm{m}$; total matrix depth beneath the floor = $2\,\mathrm{m}$; length of domain = $2\lambda = 2\,\mathrm{m}$; $\Delta p = 10^{-5}\,\mathrm{Pa}$; Re = 246; temperature = 20°C (determines water density and viscosity). Note in a) and b) that the upper portion of conduit and lower portion of matrix is not shown.

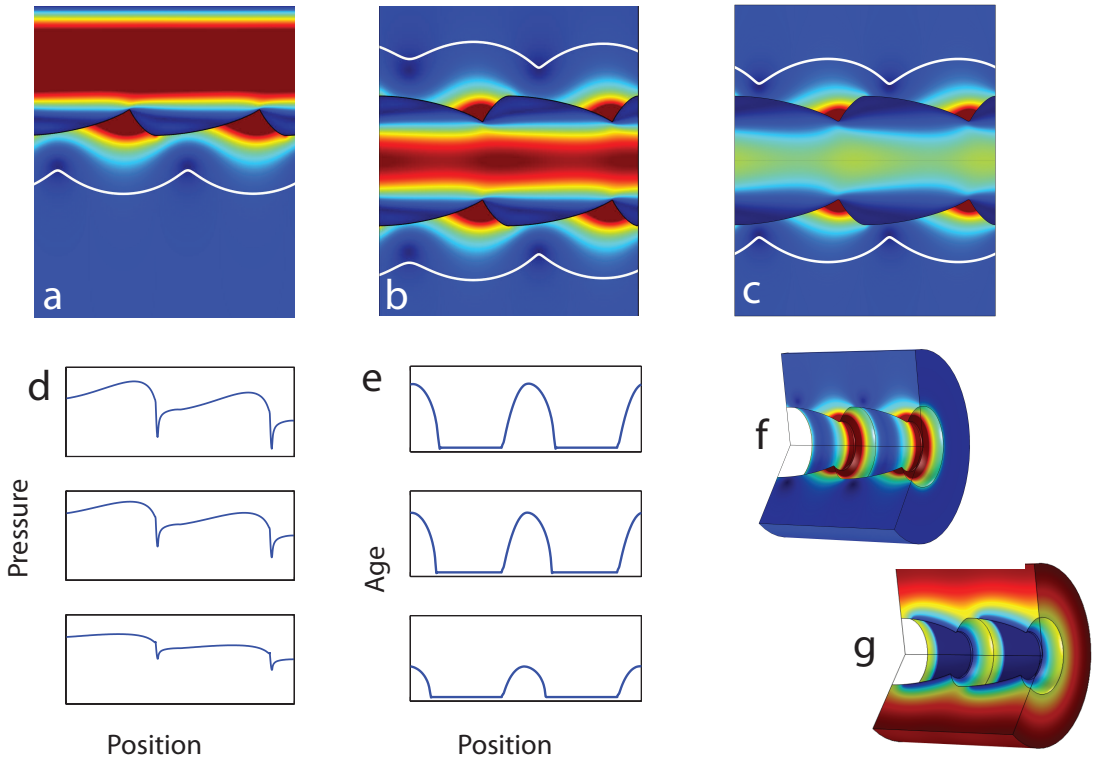

Figure 12: a) Velocity magnitude of hyporheic flow in model with a flat impermeable ceiling (as in Figure 9). Color is relative speed (red= fast, blue = slow). Streamline shows maximum depth of hyporheic flow = 0.65 m below scallop peak. $\Delta p = 10^{-5}$ Pa; Re = 246. b) Velocity magnitude of hyporheic flow in model with an impermeable ceiling with scallops. Color is relative speed (red= fast, blue = slow). Streamline shows maximum depth of hyporheic flow = 0.61 m bellow scallop peak. $\Delta p = 10^{-5}$ Pa; Re = 142. c) Velocity magnitude of hyporheic flow in model with radial symmetry. Color is relative speed (red= fast, blue = slow). Streamline shows maximum depth of hyporheic flow = 0.48 m below scallop peak. $\Delta p = 10^{-5}$ Pa; Re = 77. d) Plot of pressure along bottom of conduit: top plot is for model shown in a, middle plot for model b, lower plot for model c (x & y axis scales the same for the three plots). e) Plot of age for hyporheic water returning to the conduit: top plot is for model shown in a, middle plot for model b, lower plot for model c (x & y axis scales the same for the three plots). f) Velocity magnitude for radially symmetric model, flow velocities in the interior of conduit not shown. g) Hyporheic zone age for radially symmetric model, age in the interior of conduit not shown (red= fast, blue = slow). Color scale differs from matrix to conduit. For a, b, c, f color scales differ from matrix to conduit. The same conduit color scale is used for a, b, c. The same matrix color scale is used for a, b, c, f. Parameters: conduit diameter (measured from scallop trough for a, trough to trough for b, c = b = 1 m; scallop wave length (distance between peaks) = λ = 1 m; scallop height = H = 0.2 m; total matrix depth beneath the floor for a = 2 m, for b, c = 1 m; length of domain = 2λ = 2 m; temperature = 20°C (determines water density and viscosity).

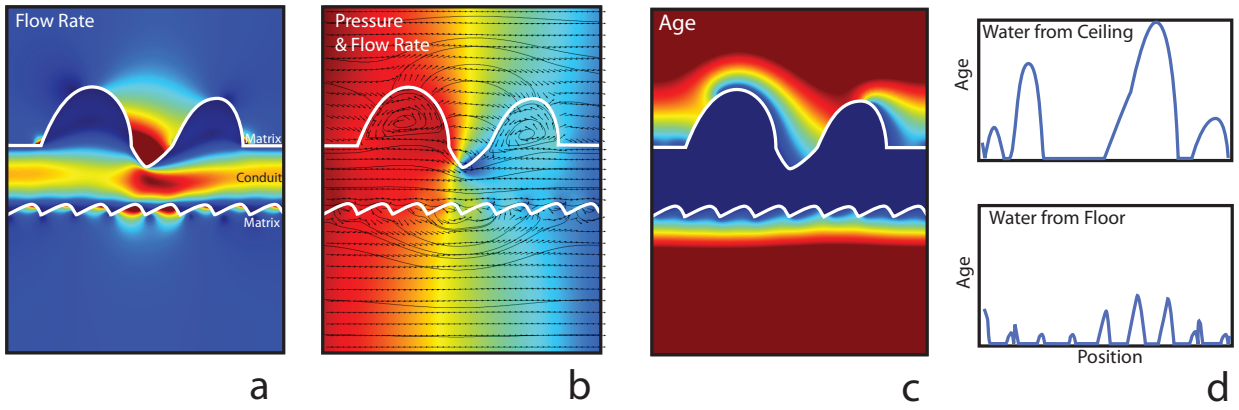

Figure 13: Model of karst hyporheic flow through the porous matrix above and below a conduit, with large cupolas along the ceiling and regularly-spaced scallops on the floor. a) Velocity magnitude. Color is relative speed (red = fast, blue = slow), color scales are different in conduit and matrix. b) Pressure distribution & flow field. Color is pressure (red = high, blue = low). Arrows show velocities. Flow paths shown in matrix and conduit. The ceiling morphology drives the hyporheic flow deeper into the matrix ceiling above the conduit than the scallops drive flow into the matrix below the floor. With a porous and morphologically complex ceiling and floor, there is an interaction between the floor and ceiling morphology that creates nested hyporheic flow paths in the matrix on the other side of the conduit. c) Relative age of hyporheic flow. Color (red= old, blue = new). d) Spatial distribution of relative residence time of returning hyporheic flow to the conduit from the ceiling (top) and floor (bottom) matrices; y-axis scales are different for top and bottom. Parameters: conduit diameter (measured from scallop trough to the top of the incoming conduit on the left) = b = 0.5 m; scallop wave length on the floor (distance between peaks) = λ = 0.25 m (0.05 m lee-side length); scallop height = H = 0.1 m; total matrix depth beneath the floor = 1 m; cupola depths = 0.40 and 0.35 m; matrix penetration into the conduit between the cupolas = 0.15 m; total matrix height above the ceiling = 1.0 m; length of domain = 2λ = 2 m; $\Delta p = 10^{-5}$ Pa; temperature = 20°C (determines water density and viscosity).